Research article

JHEP|Reports

TAK1 deficiency promotes liver injury and tumorigenesis via ferroptosis and macrophage cGAS-STING signalling

Wantong Su,[1,2,†] **Weicheng Gao,**[1,†] Rui Zhang,[1,2] Qi Wang,[1,2] Lei Li,[1,2] Qingfa Bu,[1,2] Zibo Xu,[1,2] Zheng Liu,[1,2] Mingming Wang,[1,2] Yaqing Zhu,[3,*] Guoping Wu,[1,*] Haoming Zhou,[1,2,*] Xun Wang,[1,2,*] Ling Lu[1,2,4]

[1]*Department of Plastic and Cosmetic Surgery of The Affiliated Friendship Plastic Surgery Hospital & Hepatobiliary Center of The First Affiliated Hospital, Nanjing Medical University, Nanjing, China;* [2]*Research Unit of Liver Transplantation and Transplant Immunology, Chinese Academy of Medical Sciences, Nanjing, China;* [3]*Department of Hepatobiliary Surgery, the First Affiliated Hospital of Guangzhou University of Traditional Chinese Medicine, Guangzhou, China;* [4]*Jiangsu Key Laboratory of Cancer Biomarkers, Prevention and Treatment, Collaborative Innovation Center for Cancer Personalized Medicine, Nanjing Medical University, Nanjing, China*

JHEP Reports **2023.** https://doi.org/10.1016/j.jhepr.2023.100695

Background & Aims: Oxidative stress-mediated ferroptosis and macrophage-related inflammation play an important role in various liver diseases. Here, we explored if and how hepatocyte ferroptosis regulates macrophage stimulator of interferon genes (STING) activation in the development of spontaneous liver damage, fibrosis, and tumorigenesis.

Methods: We used a transforming growth factor-beta-activated kinase 1 (TAK1) deficiency-induced model of spontaneous liver damage, fibrosis, and tumorigenesis to investigate hepatocyte ferroptosis and its impact on macrophage STING signalling. Primary hepatocytes and macrophages were used for *in vitro* experiments.

Results: Significant liver injury and increased numbers of intrahepatic M1 macrophages were found in hepatocyte-specific TAK1-deficient ($TAK1^{\Delta HEP}$) mice, peaking at 4 weeks and gradually decreasing at 8 and 12 weeks. Meanwhile, activation of STING signalling was observed in livers from $TAK1^{\Delta HEP}$ mice at 4 weeks and had decreased at 8 and 12 weeks. Treatment with a STING inhibitor promoted macrophage M2 polarisation and alleviated liver injury, fibrosis, and tumour burden. TAK1 deficiency exacerbated liver iron metabolism in mice with a high-iron diet. Moreover, consistent with the results from single-cell RNA-Seq dataset, $TAK1^{\Delta HEP}$ mice demonstrated an increased oxidative response and hepatocellular ferroptosis, which could be inhibited by reactive oxygen species scavenging. Suppression of ferroptosis by ferrostatin-1 inhibited the activation of macrophage STING signalling, leading to attenuated liver injury and fibrosis and a reduced tumour burden. Mechanistically, increased intrahepatic and serum levels of 8-hydroxydeoxyguanosine were detected in $TAK1^{\Delta HEP}$ mice, which was suppressed by ferroptosis inhibition. Treatment with 8-hydroxydeoxyguanosine antibody inhibited macrophage STING activation in $TAK1^{\Delta HEP}$ mice.

Conclusions: Hepatocellular ferroptosis-derived oxidative DNA damage promotes macrophage STING activation to facilitate the development of liver injury, fibrosis, and tumorigenesis. Inhibition of macrophage STING may represent a novel therapeutic approach for the prevention of chronic liver disease.

Impact and implications: The precise mechanism by which hepatocyte ferroptosis regulates macrophage STING activation in the progression of liver damage, fibrosis, and tumorigenesis remains unclear. Herein, we show that deletion of TAK1 in hepatocytes caused oxidative stress-mediated ferroptosis and macrophage-related inflammation in the development of spontaneous liver injury, fibrosis, and hepatocellular carcinoma.

Introduction

Ferroptosis is an iron-dependent form of regulated cell death driven by excessive phospholipid peroxidation.[1] Various types of organ injuries and degenerative pathologies are driven by ferroptosis. Excessive or defective ferroptosis contributes to tissue damage and tumorigenesis.[2] Both anti- and protumorigenic roles of ferroptosis have been reported in different models.[3] Unrestricted cell death or tissue damage may cause an inflammation-related immunosuppressive microenvironment, leading to tumour progression or recurrence.[4] Ferroptosis has also been implicated in the development and therapeutic responses of various types of tumours. The proferroptotic activity of several antitumour drugs, including sorafenib and sulfasalazine, has been revealed in preclinical models.[5]

Reactive oxygen species (ROS) represent a group of highly reactive molecules that have a role in a number of important

Keywords: TAK1; STING; Oxidative stress; Ferroptosis; Tumorigenesis.
Received 27 July 2022; received in revised form 16 January 2023; accepted 21 January 2023; available online XXX

† These authors contributed equally to this work.

* Corresponding authors. Addresses: Hepatobiliary Center of The First Affiliated Hospital, Nanjing Medical University, Nanjing, China (X. Wang, H. Zhou); Department of Plastic and Cosmetic Surgery of the Affiliated Friendship Plastic Surgery Hospital, Nanjing Medical University, Nanjing, China (G. Wu); Department of Hepatobiliary Surgery, The First Affiliated Hospital of Guangzhou University of Traditional Chinese Medicine, Guangzhou, China (Y. Zhu).
E-mail addresses: wangxun@njmu.edu.cn (X. Wang), hmzhou@njmu.edu.cn (H. Zhou), drgpwu@aliyun.com (G. Wu), doctorzhuyq@163.com (Y. Zhu).

cellular signalling pathways. The overproduction of ROS has been implicated in a variety of diseases, including cancer, inflammation, and neurodegenerative diseases.[6] Excessive accumulation of ROS can also trigger programmed cell death (PCD), of which ferroptosis is initiated by the failure of antioxidant defences, resulting in continued lipid peroxidation, eventual cell death, and release of damage-associated molecular patterns (DAMPs) to activate inflammation.[7]

The cyclic GMP-AMP synthase- (cGAS-) stimulator of interferon genes (STING) pathway has emerged as a key mediator of inflammation.[8] Beyond the vital role of cGAS-STING signalling in the antimicrobial innate immune response, emerging evidence has indicated its function in inflammatory and autoimmune diseases and antitumour immunity. Both antitumorigenic and protumorigenic functions of STING signalling have been reported, which are dependent on the specific context and stage of tumour progression.[9] DNA or cGAMP from apoptotic and necrotic malignant cells can be engulfed or transferred into the cytosol of dendritic cells and macrophages, which further activates cGAS-STING signalling and promotes the secretion of proinflammatory cytokines and chemokines and primes other immune cells, such as CD8 T cells and natural killer (NK) cells, to restrict tumorigenesis.[10] In contrast, mutation of the proto-oncogene KRAS induced chronic activation of cGAS-STING signalling, leading to nuclear factor-kappa B (NF-κB)-mediated persistent inflammation and cancer progression.[11]

Oxidative DNA damage not only contributes to genomic instability, which is a typical cancer hallmark as well as an important driving force of cancer, but also plays prominent roles in cGAS-STING pathway-related antitumour immunity or promoting inflammation-driven carcinogenesis.[12] Inflammation plays a vital role in liver injury, regeneration, fibrosis, and tumorigenesis. A low-level inflammatory response is essential for maintaining tissue homeostasis in response to potential insults such as infection, trauma, and metabolic stress.[13] Overactivation or persistent inflammation results in tissue damage, remodelling, and cancer development. Up to 20% of cancers are linked to chronic infections.[14]

Transforming growth factor-beta (TGF-β)-activated kinase 1 (TAK1) is a member of the MAP kinase kinase kinase (MAP3K) family. NF-κB and JNK activation by TAK1 plays a key role in regulating cell survival, inflammation, and tumorigenesis.[15] TAK1 is critical for the survival of both haematopoietic cells and hepatocytes. TAK1 deletions or losses can be detected in various types of human cancers and are positively associated with tumour progression and poor patient survival.[16–20] Elevated TAK1 expression and activity have also been detected in several human cancers,[21–24] including hepatocellular carcinoma (HCC),[25,26] indicating a dual role of TAK1 in regulating tumour initiation, progression, and metastasis. Mice with hepatocyte-specific deletions of TAK1 developed spontaneous liver fibrosis and hepatocarcinogenesis.[27] Therefore, further studies are needed to determine the role of TAK1 signalling in regulating liver tumour initiation, progression, metastasis, and therapeutic response.

Various types of cell death regulated by TAK1 have been reported. TAK1 deficiency triggered inflammasome activation and pyroptosis, apoptosis, and necroptosis of TLR-primed macrophages.[28] Pathogen blockade of TAK1 triggers pyroptosis of macrophages.[29] However, the precise molecular and cellular mechanisms by which TAK1 regulates liver injury, fibrosis, and tumorigenesis remain unclear.

In the present study, we investigated the interplay of TAK1 deficiency-induced hepatocellular ferroptosis in regulating macrophage STING signalling. Ferroptosis of hepatocytes promoted oxidative DNA damage to activate macrophage STING signalling, which in turn facilitated the development of spontaneous liver injury, fibrosis, and tumorigenesis in hepatocyte-specific TAK1-deficient mice. Our findings suggest a critical role of oxidative DNA damage from hepatocellular ferroptosis in regulating macrophage STING signalling during liver injury, fibrosis, and tumorigenesis. Inhibition of hepatocellular ferroptosis or the macrophage STING signalling pathway would be a promising therapeutic target for intervening in chronic liver disease.

Materials and methods

Patients and specimens

Patients with acute liver injury (ALI), fibrosis, HCC, and normal control patients (six/group) undergoing liver surgery in the First Affiliated Hospital of Nanjing Medical University Hospital were enrolled in the current study (Table S2). Liver samples were obtained from patients who underwent hepatectomy or percutaneous liver biopsy. Liver samples were collected from six patients with ALI; six patients with pathologically diagnosed liver fibrosis, and six patients with pathologically diagnosed HCC. The control individuals that were included had no history of diabetes, alcohol abuse, or viral hepatitis. Control samples were taken from normal liver tissues at the edge of resected haemangioma. All samples were kept frozen (-80 °C). Informed consent was obtained from each patient. The studies involving human participants were reviewed and approved by The Institutional Review Board of the First Affiliated Hospital of Nanjing Medical University.

Mice and treatments

TAK1-LoxP mice ($TAK1^{FL/FL}$) were crossed with hepatocyte-specific Cre mice (Alb-Cre) to generate hepatocyte-specific TAK1 knockout mice ($TAK1^{\Delta HEP}$), which were housed at GemPharmatech Co. Ltd. (Nanjing, China). All mice were on the C57BL/6 background, and their genotype was determined by PCR from tail DNA. Cre-negative animals were used as wild-type controls. The mice were maintained under specific pathogen-free conditions with free access to water and standard chow with supplements. The animal studies were performed in strict accordance with the recommendations in the protocol, which was approved by the Institutional Animal Care and Use Committee of Nanjing Medical University.

For ferrostatin-1 (Fer-1, cat# HY-100579, MedChemExpress, Monmouth Junction, NJ, USA) treatment, ferrostatin-1 (5 mg/kg body weight) or vehicle (0.9% NaCl) was administered to the mice by i.p. injection every day from 2 weeks of age to 12 weeks of age. Serum and liver samples were collected at 4, 8, and 12 weeks of age.

For C-176 (cat# HY-112906, MedChemExpress) treatment, 200 μmol of C-176 or vehicle (0.9% NaCl) was given to the mice twice a week from 2 weeks of age to 12 weeks of age. Serum and liver samples were collected at 4, 8, and 12 weeks of age, respectively.

For NAC (cat# HY-B0215, MedChemExpress) treatment, NAC (150 mg/kg body weight) or vehicle (0.9% NaCl) was administered to the mice by i.p. injection every day from 2 weeks of age to 4 weeks of age.

For anti-8-hydroxydeoxyguanosine (anti-8-OHdG) antibody (cat# GTX41980, GeneTex, CA, USA) treatment, anti-8-OHdG antibody (5 mg/kg body weight) and control IgG (5 mg/kg, cat# MAB004, R&D Systems) were administered to the mice by i.p. injection twice a week from 2 weeks of age to 4 weeks of age.

Liver function assay/biochemical assays

Mice blood was collected from mice via the inferior vena cava with a heparin-coated microhaematocrit tube and centrifugation for 15 min at 2,000 × *g* to obtain plasma. Alanine aminotransferase (ALT) and aspartate aminotransferase (AST) were measured using an automatic chemical analyser (Olympus Company AU5800, Tokyo, Japan).

Histology, immunohistochemistry, and immunofluorescence

Liver specimens were fixed in 4% paraformaldehyde for at least 24 h and then embedded in paraffin. Sections (4 μm thick) were cut for H&E, Sirius Red staining, and Perls' Prussian Blue staining.

For immunohistochemistry, formalin-fixed paraffin-embedded sections were deparaffinised and used to assess α-SMA (1:400, cat# 19245, Cell Signaling Technology, MA, USA), F4/80 (1:200, cat# 70076, Cell Signaling Technology), 8-OHdG (1:200, cat# sc-66036, Santa Cruz, USA) and Ki67 (1:400, cat# 12202, Cell Signaling Technology). Images were acquired using a microscope (Nikon Ci-E).

For immunofluorescence, liver cryosections were deposited on glass slides. After blocking with PBS containing 1% bovine serum albumin and 0.2% Triton X-100, the sections were incubated with primary antibodies, including anti-F4/80 (1:200, cat# ab6640 Abcam, USA), anti-STING (1:200, cat# 19851-1-AP, Proteintech), anti-CD68 (1:200, cat# 26042, Cell Signaling Technology), anti-iNOS (1:200, cat# 18985-1-AP, Proteintech), and anti-CD206 (1:200, cat# 18704-1-AP, Proteintech) at 4 °C overnight. The secondary antibodies were conjugated with Alexa 488 (1:200, cat# 4408, or # 4412, Cell Signaling Technology) or Alexa 594 (1:200, cat# 8889, Cell Signaling Technology), and the nuclei were counterstained with DAPI.

Cell isolation and treatment

Hepatocytes from TAK1$^{FL/FL}$ and TAK1$^{\Delta HEP}$ mice were isolated by two-step collagenase perfusion. In brief, livers were perfused *in situ* via the portal vein with 50 ml warmed (37 °C) HBSS (Ca^{2+} and Mg^{2+} free) containing EGTA (0.5 M), followed by collagenase IV (Sigma, Saint Louis, MO, USA, 0.05% w/v, dissolved in HBSS with Ca^{2+} and Mg^{2+}). Perfused livers were dissected and teased through 70-mm nylon mesh cell strainers. Hepatocytes were separated by an initial centrifugation at 50 × *g* for 3 min (the supernatant was collected for non-parenchymal cell isolation later, [NPC fraction]). The hepatocyte pellets were resuspended in DMEM (including 10% foetal bovine serum, 10 mM HEPES, and 1% pen/strep) and centrifuged again. Then, the pellets were seeded into collagen-precoated plates.

For primary macrophage isolation, the collected NPC fraction was centrifuged at 500 × *g* for 8 min at 4 °C. Then, 25% Percoll was placed carefully on top of the 50% Percoll layer. The pellets were pooled, and the NPC suspension was carefully and slowly placed on top of the 25% density-gradient solution layer in such a way that a clear separation of the two layers was achieved. Then, centrifugation at 800 × *g* was performed for 15 min at 4 °C without braking. The NPCs were located in the interphase between the 25% and 50% density gradient layers. The cells were washed with PBS, centrifuged at 500 × *g* for 8 min at 4 °C, and then seeded for 30 min to increase macrophage purity. Non-adherent cells were removed by replacing the culture medium. Macrophages were cultured for 6 h *in vitro*. Cells were collected for further experiments.

To study the effects of STING inhibitors on macrophage polarisation, primary liver macrophages were pretreated for 1 h with C-176 (0.5 μM) or vehicle and co-cultured with TAK1$^{FL/FL}$ and TAK1$^{\Delta HEP}$ primary hepatocytes for 6 h. Primary macrophages were collected for Western blot analysis and RT-qPCR.

For co-culture study, isolated primary hepatocytes from TAK1$^{FL/FL}$ or TAK1$^{\Delta HEP}$ mice were pretreated with or without Fer-1 (2 μM, MedChemExpress) and then co-cultured with primary macrophages for 12 h. Cells were harvested for Western blot analysis.

Data collection and gene set enrichment analysis

The data analysed in this study were obtained from the Gene Expression Omnibus (GEO) at GSE148859. Then, the dataset containing TAK1$^{FL/FL}$ and TAK1$^{\Delta HEP}$ mice was selected for subsequent analysis, and it included 18,495 cells. Hepatocytes were reclustered by using the CCA algorithm of Seurat (version 4.0.3). Downstream analysis was performed using Seurat (version 4.0.3) and the R package (R Foundation for Statistical Computing, Vienna, Austria) designed for single-cell gene expression datasets. Differentially expressed genes (cluster markers) were determined using the function FindAllMarkers of Seurat. Then, gene set enrichment analysis was implemented using the package clusterProfiler (version 3.16.1) with these genes, and a value of p <0.05 was set as the threshold to determine statistically significant enrichment of the gene sets. FerrDb was used to analyse hepatocyte ferroptosis-related genes.[30] The ferroptosis gene set enrichment score was determined with the VISION v3.0.0 R package according to instructions provided on GitHub (https://github.com/YosefLab/VISION) using ferroptosis gene sets obtained from the Molecular Signatures Database.[31] The Wilcoxon rank sum test was used to compare the gene expression between TAK1$^{FL/FL}$ macrophages and TAK1$^{\Delta HEP}$ macrophages, and a value of p <0.05 was considered statistically significant.

Transmission electron microscopy

Liver tissues were fixed with 2% glutaraldehyde in 0.1 M phosphate buffer (pH 7.4) followed by 1% OsO_4. After dehydration, thin sections were stained with uranyl acetate and lead citrate for observation under an FEI Tecnai G2 electron microscope.

Measurement of malondialdehyde, 4-hydroxynonenal, superoxide dismutase, and the ratio of glutathione/glutathione disulfide

Liver sample malondialdehyde (MDA), 4-hydroxynonenal (4-HNE), superoxide dismutase (SOD) levels and glutathione/glutathione disulfide (GSH/GSSG) ratio were measured using an MDA Assay kit (Cat#S0131S, Beyotime, China), Lipid Peroxidation (4-HNE) Assay Kit (cat#ab238538, Abcam), SOD Assay Kit (Cat#S0109, Beyotime), and GSH/GSSG Assay Kit (Cat#S0053, Beyotime), respectively, in accordance with the manufacturer's instructions.

Measurement of serum and hepatic levels of ferritin and hepcidin

Serum and hepatic levels of ferritin and hepcidin were measured using the Mouse Ferritin ELISA Kit (cat#ab157713, Abcam) and

Mouse Hepcidin ELISA Kit (cat#ab285280, Abcam) respectively, in accordance with the manufacturer's instructions.

Dihydroethidium and 2′,7′-dichlorodihydrofluorescein diacetate staining

To measure *in situ* ROS levels, frozen liver sections were incubated with dihydroethidium (DHE; 3 μM, Invitrogen) and 2′,7′-dichlorodihydrofluorescein diacetate (DCFDA) (5 μM, Molecular Probes) at 37 °C for 30 min protected from light and were examined under a fluorescence microscope.

Measurement of C11-BODIPY content

Primary hepatocytes from TAK1$^{FL/FL}$ and TAK1$^{\Delta HEP}$ mice were fixed with 4% paraformaldehyde and permeabilised with 0.2% Triton X-100. After washing with PBS, the hepatocytes were incubated with BODIPY^{TM} 581/591 C11 (Invitrogen^{TM} D3861, 5 μmol/L) for 30 min at 37 °C. DAPI was used to stain cell nuclei. Images were obtained on a Zeiss AxioObserver Z1 confocal microscope.

Measurement of serum and culture media levels of 8-hydroxydeoxyguanosine

The concentration of serum and culture media (8-OHdG) were determined by an 8-Hydroxydeoxyguanosine Assay Kit (cat# H165, Nanjing Jiancheng, China) according to the manufacturer's instructions.

Quantitative real-time PCR

Total RNA was isolated from liver tissue using TRIzol and subjected to reverse transcription with the Takara reverse transcriptase kit (Takara Bio, Tokyo, Japan). A SYBR RT–PCR Kit (Takara) was used for reverse transcription quantitative PCR (RT-qPCR) analysis. The PCR primer sequences are listed in Table S1. The expression of the respective genes was normalised to that of GAPDH as an internal control.

Western blotting analysis

Proteins from the liver tissue and macrophages were separated by 10–12% SDS-PAGE and transferred onto polyvinylidene difluoride membranes. After blocking, the polyvinylidene difluoride membranes were incubated overnight at 4 °C with primary antibodies, including cGAS antibody (1:1000, cat# 31659, CST), STING antibody (1:1000, cat# 13647, CST), phospho-TBK1 antibody (1:1000, cat# 5483, CST) phospho-STING antibody (1:1000, cat#72971, CST), phospho-IRF3 antibody (1:1000, cat#29047, CST), phospho-NF-κB antibody (1:1000, cat#3033, CST), α-SMA antibody (1:1000, cat# 19245, CST), TAK1 antibody (1:1000, cat# ab109526 Abcam), GPX4 antibody (1:1000, cat# ab125066, Abcam), OGG1 antibody (1:1000, cat# 15125-1-AP, Proteintech), GAPDH antibody (1:1000, cat# 5174, CST), NRF2 antibody (1:1000, cat# 12721, CST), Lamin B1 antibody (1:1000, cat# 12586, CST), phospho-STAT1 antibody (1:1000, cat# 9167, CST), Arginase-1 (ARG-1) antibody (1:1000, cat# 93668, CST), NLRP3 antibody (1:1000, cat# 15101, CST) and incubated with horseradish peroxidase-conjugated secondary antibody at room temperature. The signals were detected using chemiluminescence horseradish peroxidase substrate (WBKL0100; Millipore Sigma) and an enhanced chemiluminescence detection system. Proteins in Western blots were quantified in optical density units with ImageJ software (National Institutes of Health, USA).

Statistical analysis

Two-group comparisons were performed using the Mann–Whitney *U* test or Wilcoxon rank sum test, whereas for more than two groups, Kruskal–Wallis tests were performed. Statistical analysis was performed using GraphPad Prism Version 7.0 (GraphPad Software, San Diego, CA, USA). Data were expressed as mean ± SEM and a value of p <0.05 was regarded as statistically significant.

Results

Deletion of TAK1 in hepatocytes caused the development of spontaneous liver injury, fibrosis, and hepatocellular carcinoma

Spontaneous liver injury, fibrosis, and hepatocellular carcinoma have been found previously in mice with TAK1 deficiency in hepatocytes.[32] To study the precise role and mechanism of TAK1 in hepatocytes, TAK1$^{\Delta HEP}$ mice were generated by crossing TAK1$^{flox/flox}$ mice with albumin-Cre mice. Protein expression of TAK1 in isolated hepatocytes and liver nonparenchymal cells confirmed the efficient and specific deletion of TAK1 in TAK1$^{\Delta HEP}$ mice (Fig. 1A). Liver injury was found in TAK1$^{\Delta HEP}$ mice early at 4 weeks of age and decreased by 8 and 12 weeks of age, as indicated by significantly increased serum ALT and AST levels (Fig. 1B and C) and liver pathologic examination (Fig. 1D). Liver fibrosis was detected in TAK1$^{\Delta HEP}$ mice from 4 weeks of age, as shown by immunostaining with Sirius Red (Fig. 1E) and α-SMA (Fig. 1F). To further study the mechanism of hepatic TAK1 in affecting liver fibrosis, we conducted a macrophage-hepatic stellate cells (HSCs) co-culture experiment. Primary mouse HSCs were incubated with TAK1$^{FL/FL}$ or TAK1$^{\Delta HEP}$ primary macrophage conditioned media (CM) for 24 h (Fig. S1A). The α-SMA protein expression indicated that CM from TAK1$^{\Delta HEP}$ primary macrophage markedly promote the activation of HSCs (Fig. S1B). The gene expression of fibrotic markers (TGFβ-1, Colla1, Timp1) further confirmed these findings (Fig. S1C). Moreover, TAK1$^{\Delta HEP}$ mice developed liver tumour nodules at 12 weeks old and had an increased liver-to-body weight ratio from 4 to 12 weeks old (Fig. 1G and H). These results confirmed that deletion of TAK1 in hepatocytes resulted in spontaneous development of liver injury, fibrosis, and HCC.

Hepatocyte-specific TAK1 deficiency regulated macrophage polarisation at different stages of liver injury, fibrosis, and tumorigenesis in TAK1$^{\Delta HEP}$ mice

Macrophages play an important role in regulating various types of liver diseases. Therefore, we determined whether macrophages function in regulating liver injury, fibrosis, and tumorigenesis in TAK1$^{\Delta HEP}$ mice. Significantly increased numbers of F4/80+ macrophages were detected in the livers of TAK1$^{\Delta HEP}$ mice, peaking at 4 weeks and gradually decreasing by 8 and 12 weeks (Fig. 2A). Macrophage M1/M2 polarisation was evaluated at different time points by Western blotting of p-STAT1 and Arg-1 (Fig. 2B), immunostaining of iNOS and CD206 (Fig. 2C) and gene induction of iNOS, CD86, CD206, CD163 (Fig. 2D and E), and inflammatory cytokines (Fig. 2F and G). The results showed that intrahepatic macrophages of TAK1$^{\Delta HEP}$ mice were predominantly the M1 phenotype at 4 weeks and gradually shifted to the M2 phenotype at 8 and 12 weeks. These findings indicated that hepatocyte TAK1 deficiency promoted intrahepatic macrophage M1 polarisation during liver injury, M2 polarisation during fibrosis, and tumorigenesis.

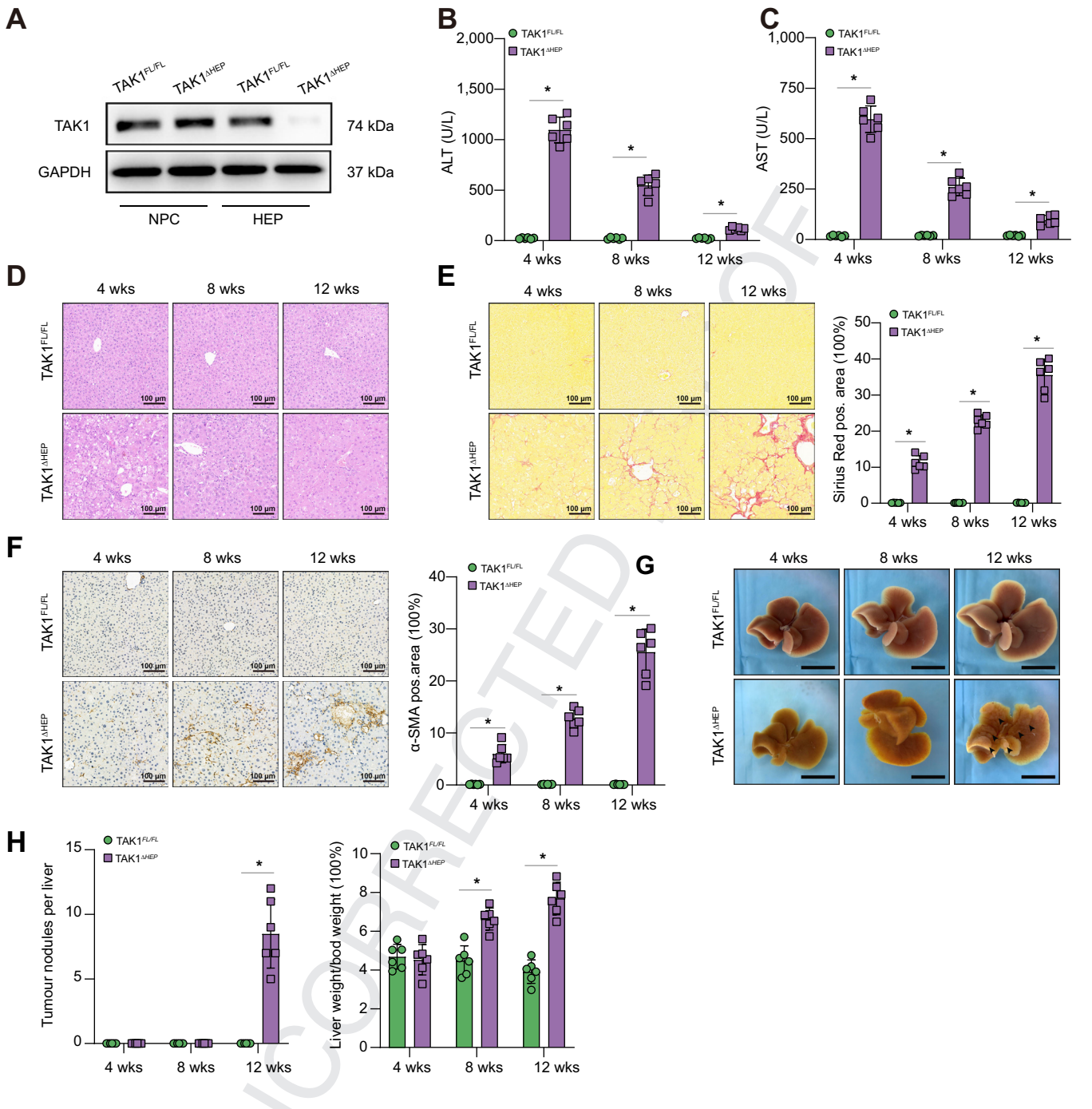

Fig. 1. Deletion of TAK1 in hepatocytes caused the development of spontaneous liver injury, fibrosis, and hepatocellular carcinoma. (A) Specific deletion of TAK1 in hepatocytes was confirmed by Western blot analysis. Liver function and histological staining were performed at three different time points. (B, C) Serum ALT and AST levels; n = 6/group. (D) Representative H&E staining, (E) Sirius Red staining, and (F) immunohistochemistry images of α-SMA in liver sections (200 × magnification, scale bars = 100 μm, n = six/group). (G) Representative liver images from different-week-old mice. Arrowheads denote tumours (scale bars = 1 cm). (H) Tumour nodules number and the ratio of liver-to-body weight. Data are presented as the mean ± SEM (n = 6). *p <0.05 Mann–Whitney U test. ALT, alanine aminotransferase; AST, aspartate aminotransferase; GAPDH, glyceraldehyde-3-phosphate dehydrogenase; HEP, hepatocytes; NPC: nonparenchymal cells; TAK1, transforming growth factor-beta-activated kinase 1; w, weeks.

Macrophage STING signalling contributed to liver injury, fibrosis, and tumorigenesis in TAK1$^{\Delta HEP}$ mice

Macrophage STING signalling has been implicated in various liver diseases.[33] To investigate the changes in macrophage STING signalling affected by TAK1 depletion in hepatocytes, graph-based clustering with Seurat was performed on the single-cell RNA-Seq dataset (GSE148859). As STING and TBK1 are important components of the STING signalling pathway, we evaluated the expression of these two genes by bioinformatic analysis. Gene expression violin plots and feature plots of all clusters were constructed using the Seurat VlnPlot and featureplot function with the parameter pt. size = 0. The results showed that STING

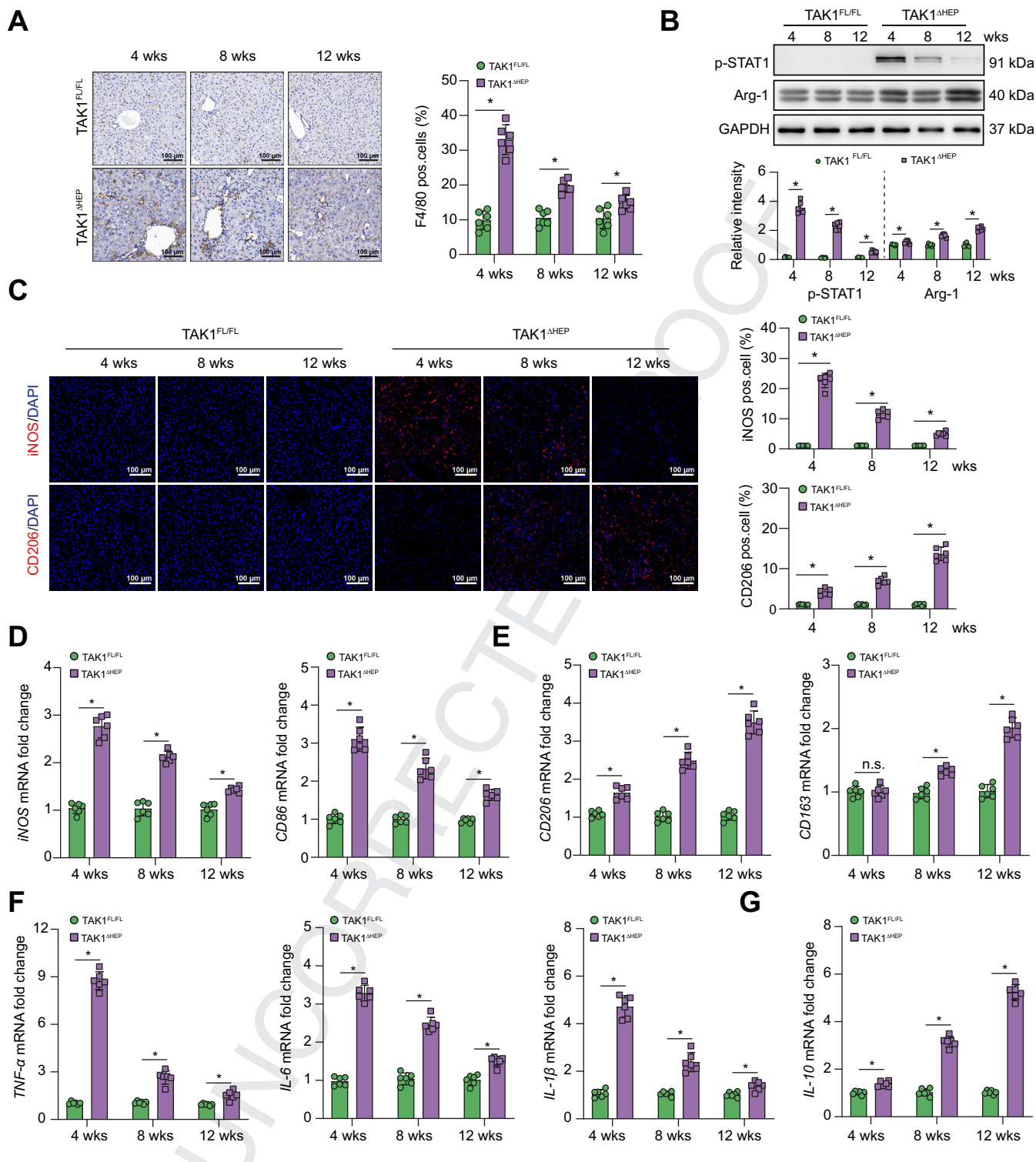

Fig. 2. Hepatocyte-specific TAK1 deficiency regulated macrophage polarisation at different stages. Histological staining and RT-qPCR were performed using TAK1$^{FL/FL}$ and TAK1$^{\Delta HEP}$ samples from mice of different ages. (A) Representative immunohistochemistry staining of F4/80 in liver tissues (200 × magnification, scale bars = 100 μm). (B) The protein levels of p-STAT1, Arg-1, and GAPDH in liver tissues. (C) Representative dual immunofluorescence staining for iNOS or CD206 with DAPI (200 × magnification, scale bars = 100 μm). (D, E) The gene expression of iNOS, CD86, CD206, and CD163 in liver tissues. (F, G) The gene expression of TNF-α, IL-6, IL-1β, and IL-10. Data are presented as the mean ± SEM (n = 6). ns, not significant, *p <0.05 Mann–Whitney U test. GAPDH, glyceraldehyde-3-phosphate dehydrogenase; TAK1, transforming growth factor-beta-activated kinase 1; TNF-α, tumour necrosis factor-alpha; w, weeks.

expression was predominantly observed in endothelial cells, macrophages and plasma cells, whereas TBK1 was predominantly expressed in endothelial cells, hepatocytes, macrophages, T cells, and NK cells in TAK1$^{FL/FL}$ mice (Fig. S2A and B). Moreover, TAK1$^{\Delta HEP}$ mice showed higher expression levels of STING and TBK1 in macrophages (Fig. S2C and Fig. 3A), suggesting that TAK1

deficiency in hepatocytes upregulated STING signalling in macrophages. In addition, some other types of liver parenchymal and nonparenchymal cells, such as macrophages and endothelial cells, also demonstrated increased STING activation in TAK1-deficient mice. Interestingly, previous studies have shown the important role of STING signalling in regulating inflammation and cell death in endothelial cells.[34,35] It would be interesting to investigate the role of STING signalling in other liver cells of TAK1$^{\Delta HEP}$ mice in future studies.

Primary hepatocytes and macrophages were isolated to further check STING expression in both cell lines by Western blotting. The results showed that hepatocytes lacked STING expression compared with macrophages (Fig. 3B). The mRNA expression levels of interferon-beta (IFN-β) and NF-κB, two major target genes downstream of STING activation,[36] showed a significant increase at 4 weeks and decreased at 8 and 12 weeks (Fig. 3C and D). Consistently, Western blotting results showed that the cGAS-STING signalling pathway was significantly activated in livers from TAK1$^{\Delta HEP}$ mice at 4 weeks and decreased at 8 and 12 weeks (Fig. 3E).

To further determine the essential role of macrophage STING signalling, the STING inhibitor C-176 was used to block STING activation. We previously found that STING regulated NLRP3 signalling in M1 macrophage polarisation.[37,38] *In vitro*, STING inhibition by its antagonist promoted M2 polarisation but inhibited M1 polarisation of macrophages (Fig. S3A-D). *In vivo*, treatment with the STING inhibitor alleviated liver injury and inflammation at 4 weeks (Fig. 4A–E) and attenuated liver fibrosis at 8 weeks (Fig. 4F and G). In addition, *in vivo* STING inhibition resulted in reduced tumour burden and restored liver-to-body weight ratio in TAK1$^{\Delta HEP}$ mice (Fig. 4H and I), which provided more evidence about the relationship between macrophage STING signalling and HCC progression. Together, these results suggested that macrophage STING signalling contributed to the disease progression of TAK1$^{\Delta HEP}$ mice.

TAK1 deficiency promoted ferroptosis of hepatocytes by inducing oxidative stress and disordered iron metabolism

We next determined the type of hepatocellular cell death caused by TAK1 depletion. The viability of primary hepatocytes was

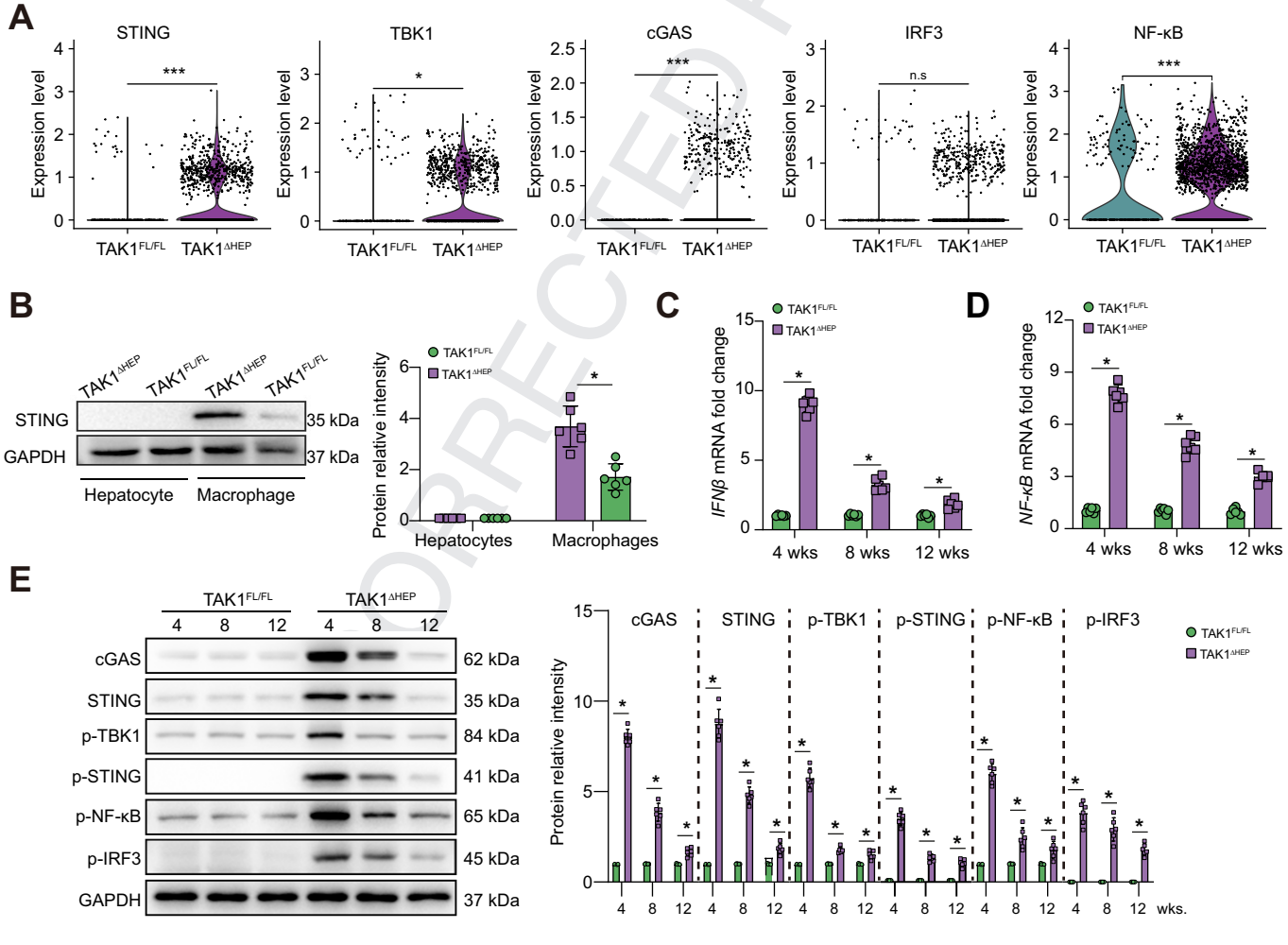

Fig. 3. Macrophage STING signalling contributed to liver injury, fibrosis, and tumorigenesis in TAK1$^{\Delta HEP}$ mice. (A) Violin plot from the single-cell RNA-Seq dataset (GSE148859) depicting higher expression of *STING*, *TBK1*, *cGAS*, *IRF3*, and *NF-κB* in the TAK1$^{\Delta HEP}$group, n.s., not significant, *p <0.05, ***p <0.001 Wilcoxon rank sum test. (B) Western blot was performed to analyse the levels of STING in primary hepatocytes and macrophages isolated from TAK1$^{FL/FL}$ and TAK1$^{\Delta HEP}$ mice. (C, D) The gene expression of IFN-β and NF-κB in primary mouse macrophages. (E) The protein levels of cGAS-STING signalling in primary mouse macrophages. Data are presented as the mean ± SEM (n = 6). *p <0.05, Mann–Whitney *U* test. cGAS, cyclic GMP-AMP synthase; GAPDH, glyceraldehyde-3-phosphate dehydrogenase; IFN-β, interferon-beta; NF-κB, nuclear factor-kappa B; STING, stimulator of interferon genes; TAK1, transforming growth factor-beta-activated kinase 1; w, weeks.

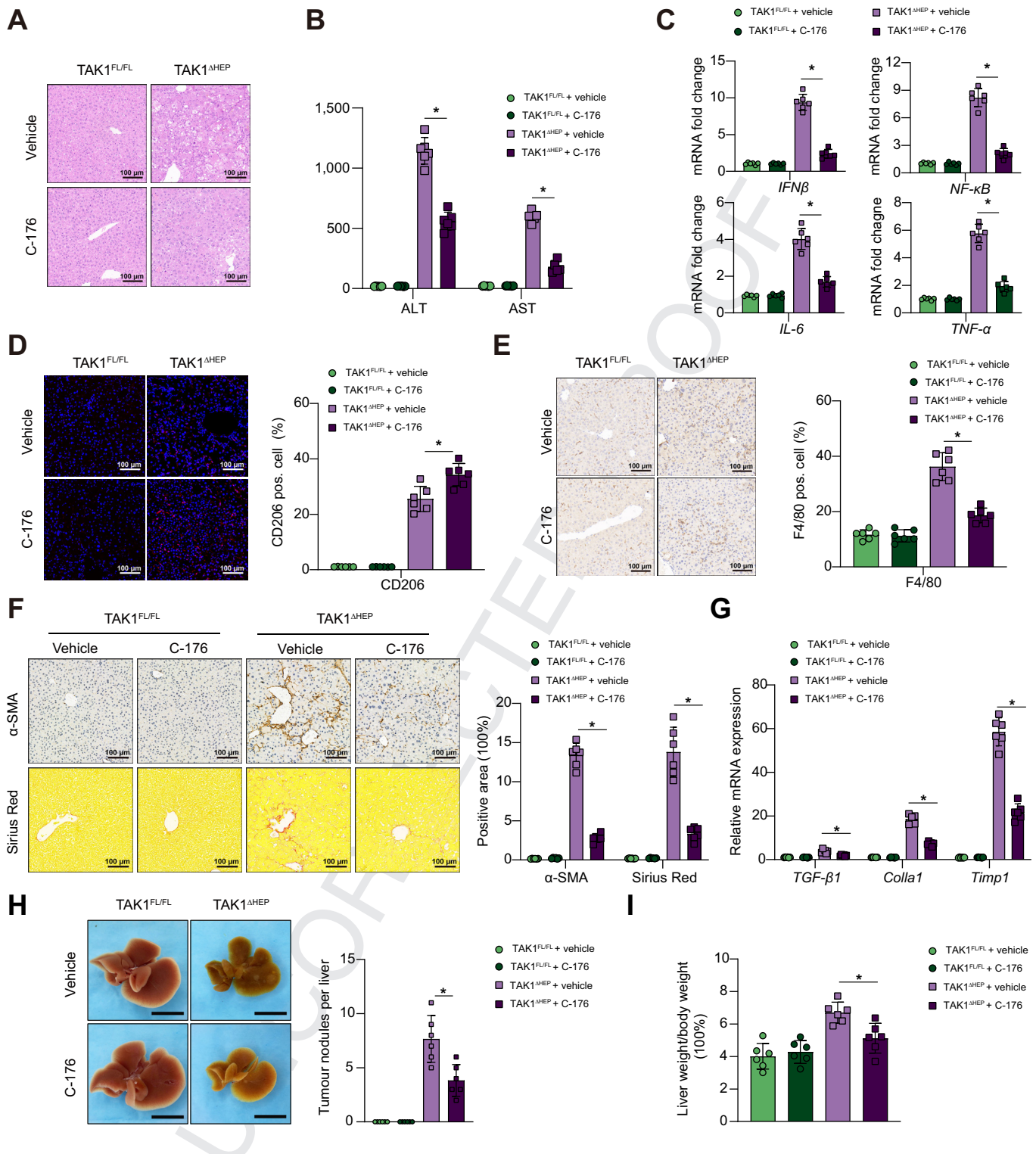

Fig. 4. STING inhibitor attenuates hepatic inflammation, injury, and fibrosis in the early stage. TAK1$^{FL/FL}$ and TAK1$^{\Delta HEP}$ mice were treated with i.p. injections of C-176 at a dose of 200 μmol or vehicle twice a week from 2 weeks of age. At 4 weeks of age, (A) liver and serum samples were collected for H&E staining (200 × magnification, scale bars = 100 μm, n = six/group), (B) ALT/AST measurement, (C) and RT-qPCR analysis for the expression of *IFN-β, NF-κB, IL-6*, and *TNF-α*. (D) Dual immunofluorescence staining for CD206 with DAPI (200 × magnification, scale bars = 100 μm) and (E) immunohistochemistry staining of F4/80 in liver tissues (200 × magnification, scale bars=100 μm) to evaluate inflammation; By 8 weeks of age, (F) liver sections were stained for F4/80, α-SMA and Sirius Red (200 × magnification, scale bars=100 μm, n = six/group) and (G) RT-qPCR analysis of *TGF-β, Colla1*, and *Timp1*. By 12 weeks of age, liver tissues were collected to assess tumour burden (H) and determine the liver-to-body weight ratio (I). Data are presented as the mean ± SEM (n = 6). *p <0.05 Mann–Whitney *U* test. ALT, alanine aminotransferase; AST, aspartate aminotransferase; IFN-β, interferon-beta; NF-κB, nuclear factor-kappa B; STING, stimulator of interferon genes; TAK1, transforming growth factor-beta-activated kinase 1; TNF-α, tumour necrosis factor-alpha.

checked, and results of CCK-8 and cellular supernatant lactate dehydrogenase level showed that TAK1 deficiency decreased hepatocytes viability (Fig. S4A and B). Graph-based clustering with Seurat on the single-cell RNA-Seq dataset (GSE148859) showed that all isolated cells were grouped into 13 distinct clusters (Fig. 5A). Based on the cell annotation in the study by Tan *et al.*,[39] we reclustered hepatocytes from TAK1$^{FL/FL}$ and TAK1$^{\Delta HEP}$ mice into 11 clusters (Fig. 5B and C), of which the vast majority of hepatocytes in Cluster 7 belonged to TAK1$^{\Delta HEP}$ mouse livers. As shown in Fig. 5D of the KEGG enrichment analysis, Cluster 7 differentially expressed genes (Table S3) were mainly enriched in the ferroptosis and apoptosis signalling pathways. However, no significant difference was found in the necroptosis signalling pathway. These results suggested that, in addition to

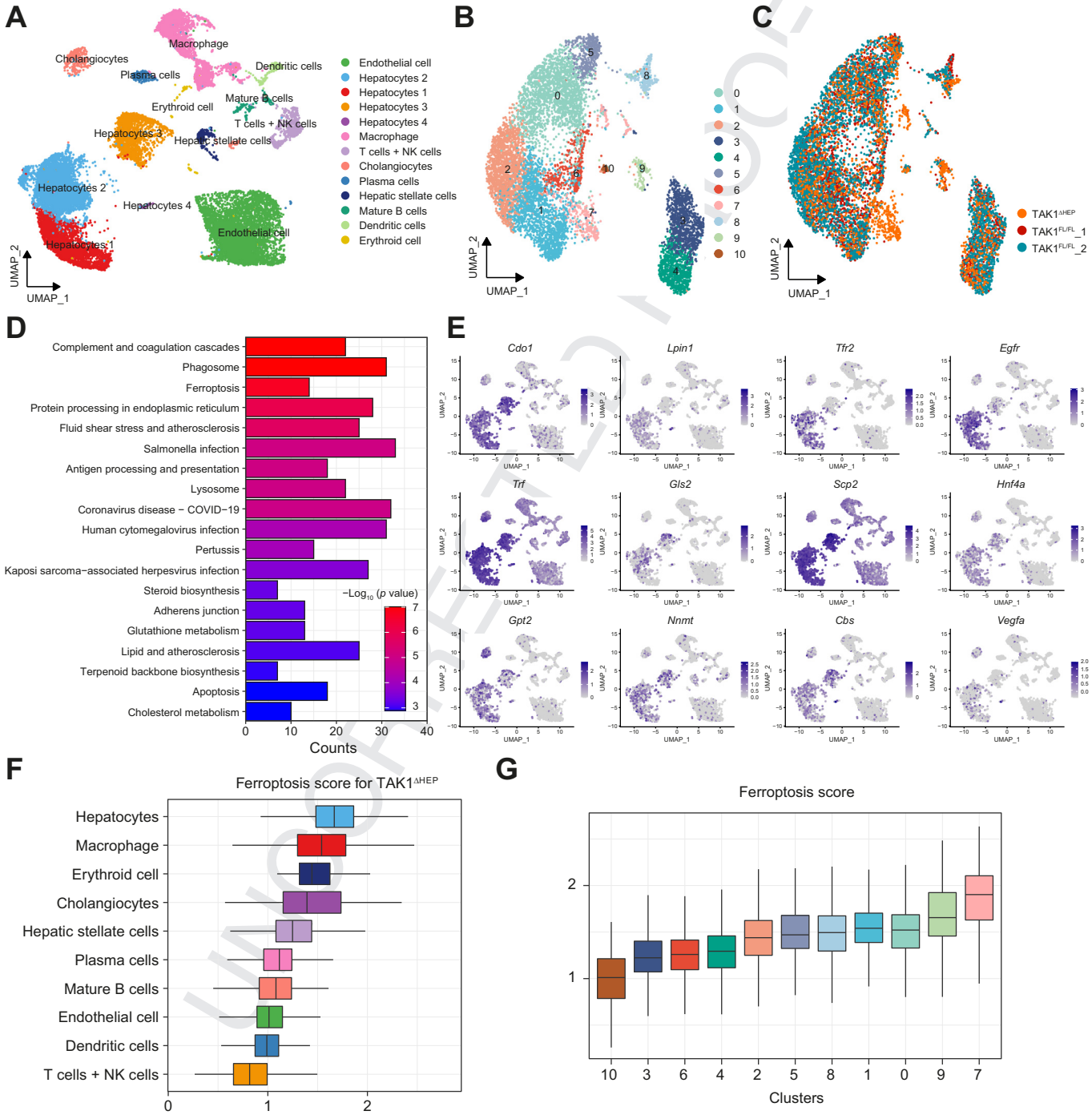

Fig. 5. ScRNA-seq data analysis of livers with TAK1 deficiency and TAK1 floxed mice. (A) UMAP visualisation of single cells profiled in the dataset (from GEO at GSE148859). (B, C) Hepatocyte reclustering analysis. (D) Enrichment analysis of most DEGs of reclustered hepatocytes. (E) Representative gene expression and distribution of ferroptosis marker genes for each population in UMAP plots. (F, G) Ferroptosis geneset enrichment scores were performed for all cell types and all reclusters of hepatocytes. DEGs, differentially expressed genes; GEO, Gene Expression Omnibus; NK cells, natural killer cells; TAK1, transforming growth factor-beta-activated kinase 1; UMAP, uniform manifold approximation and projection.

apoptosis, ferroptosis would also be one of the important forms of hepatocyte cell death caused by TAK1 deficiency. FerrDb was used to analyse hepatocyte ferroptosis-related genes. Ferroptosis marker gene expression and distribution for each population in UMAP (uniform manifold approximation and projection) plots showed that these genes were upregulated predominantly in hepatocytes compared with other cell types (Fig. 5E). In addition, we also evaluated ferroptosis scores in various types of hepatic cells and the highest scores were found in hepatocytes (Fig. 5F). Moreover, among the 11 clusters of hepatocytes, Cluster 7 hepatocytes had the highest ferroptosis scores (Fig. 5G).

Moreover, KEGG pathway analysis showed that some ROS-related pathways were involved in TAK1-deficient hepatocytes, including glutathione metabolism, fatty acid biosynthesis, and fatty acid metabolism. Features of ferroptosis, including mitochondrial volume reduction, increased bilayer membrane density, and rupture of the outer mitochondrial membrane, were found by transmission electron microscopy (TEM) in TAK1-deficient hepatocytes (Fig. 6A). Iron metabolism disorders is also an important characteristic of ferroptosis. Increased hepatic iron accumulation was found in livers from TAK1$^{\Delta HEP}$ mice, as shown by Prussian Blue staining (Fig. 6B). Elevated levels of ferritin but decreased levels of hepcidin in both liver tissues and serum were found in TAK1$^{\Delta HEP}$ mice (Fig. 6C). These results further suggested dysregulated iron metabolism in TAK1$^{\Delta HEP}$ mice. We further evaluated liver injury and inflammation in mice treated with a high-iron diet or normal diet. The results showed that treatment with an iron-rich diet increased liver injury and inflammation in TAK1$^{\Delta HEP}$ mice, as shown by serum ALT and AST levels and H&E and F4/80 staining of liver tissues (Fig. S5A–C).

TAK1-deficient hepatocytes also demonstrated accumulation of lipid ROS products, which were labelled with the fluorescent probe C11-BODIPY (581/591) (Fig. 6D). Increased lipid peroxidation and decreased antioxidant activity were found in livers from TAK1$^{\Delta HEP}$ mice, as shown by MDA, 4-HNE, and SOD expression and the GSH/GSSG ratio (Fig. 6E and F). Transcription factor nuclear factor erythroid 2-related factor 2 (NRF2) is a key player in antioxidant defence. NRF2 and its responsive genes, such as NQO1, GSTP1, and GCLC, were all upregulated in TAK1-deficient livers, suggesting enhanced NRF2 activity (Fig. 6G). The NRF2 nuclear translocation was also evaluated by Western blotting. Protein levels of NRF2 were gradually increased in nuclear but decreased in cytoplasm over the different time points, indicating sustained translocation of NRF2 to the nucleus in TAK1-deficient hepatocytes (Fig. 6H). As the role of GPX4 in ferroptosis is widely described, we measured the expression of GPX4 protein. Results showed that GPX4 expression was increased in TAK1-deficient liver tissue (Fig. S6A), possibly as a result of a compensatory antioxidant response against TAK1-deficiency-induced imbalance ROS. Moreover, ROS inhibition by NAC effectively suppressed oxidative stress in hepatocytes, ferroptosis, and liver injury (Fig. 6I–K). These results suggested that TAK1 deficiency promoted ferroptosis of hepatocytes by inducing oxidative stress and disordered iron metabolism.

Inhibition of hepatocellular ferroptosis decreased macrophage STING activation and suppressed liver injury, fibrosis, and tumorigenesis in TAK1$^{\Delta HEP}$ mice

Ferrostatin-1 (Fer-1), a specific inhibitor of ferroptosis, was used to evaluate the role of ferroptosis in regulating liver injury, fibrosis, and tumour development caused by TAK1 deficiency. Consequently, suppression of hepatocellular ferroptosis significantly inhibited the activation of macrophage STING signalling, as evidenced by fewer F4/80 and STING double-positive cells (Fig. 7A) and decreased protein levels of cGAS-STING signal pathway (Fig. 7B and C). Moreover, suppression of ferroptosis by Fer-1 effectively decreased liver injury (Fig. 7D) and liver fibrosis (Fig. 7E). TAK1$^{\Delta HEP}$ mice treated with Fer-1 also showed decreased cell proliferation and a reduced tumour burden (Fig. 7F and G). Overall, we found that TAK1 depletion in hepatocytes promoted macrophage STING activation to facilitate liver injury, fibrosis, and tumorigenesis by inducing hepatocellular ferroptosis, suggesting a therapeutic role for the suppression of macrophage STING activation or hepatocellular ferroptosis in liver disease.

Hepatocyte ferroptosis promoted oxidative DNA damage to activate macrophage cGAS-STING signalling

To investigate whether macrophage STING activation was caused by oxidative DNA damage from injured/damaged hepatocytes, we measured the expression of 8-OHdG, a marker of oxidative DNA damage, in both livers and serum from TAK1$^{\Delta HEP}$ mice. The results showed that the levels of hepatic and serum 8-OHdG were suppressed by Fer-1 treatment (Fig. 8A and B). Additionally, 8-oxoguanine DNA glycosylase 1 (OGG1) expression was increased in TAK1 deficiency liver tissue (Fig. S6A), which is the major DNA glycosylase in the repairment of damaged DNA bases. Moreover, 8-OHdG levels of cellular supernatant from TAK1-deleted hepatocytes had higher level of oxidative damaged DNA release (Fig. 8C). Isolated primary hepatocytes from TAK1$^{FL/FL}$ or TAK1$^{\Delta HEP}$ mice were pretreated with or without Fer-1 and then co-cultured with primary liver macrophages for 12 h (Fig. 8D). As shown in Fig. 8E, Fer-1 pretreatment significantly suppressed the activation of cGAS-STING signalling in primary liver macrophages co-cultured with TAK1-deficient hepatocytes. Moreover, *in vivo* treatment with an anti-8-OHG antibody effectively suppressed macrophage cGAS-STING signal activation (Fig. 8F) and decreased the gene expression of IFN-β, IL-6, tumour necrosis factor-alpha (TNF-α), and iNOS (Fig. 8G) in TAK1$^{\Delta HEP}$ mice. In addition, anti-8-OHdG-treated TAK1$^{\Delta HEP}$ mice also showed attenuated liver injury (Fig. 8H and I). Taken together, these findings indicated that oxidative DNA damage caused by hepatocyte ferroptosis promoted macrophage cGAS-STING activation signalling and intrahepatic inflammation (Fig. 8J).

Macrophage STING expression in patients with ALI, fibrosis, and HCC

Finally, we evaluated macrophage STING activation in patients with ALI, fibrosis, and HCC. Liver tissues from patients with ALI, fibrosis, or HCC, and normal controls were collected, and STING expression was analysed. Significantly increased protein levels of STING were found in liver tissues from patients with ALI, fibrosis, and HCC (Fig. S7A). Moreover, positive STING staining was observed in CD68-positive macrophages (Fig. S7B). These data suggest the critical role of macrophage STING signalling in the pathogenesis of ALI, fibrosis, and HCC in humans.

Discussion

The interplay between hepatic parenchymal cell death and macrophage-related inflammation plays a vital role in various liver diseases.[40] However, the underlying mechanism by which hepatocellular ferroptosis regulates macrophage STING

FLA 5.6.0 DTD ■ JHEPR100695_proof ■ 9 March 2023 ■ 5:04 am ■ ce

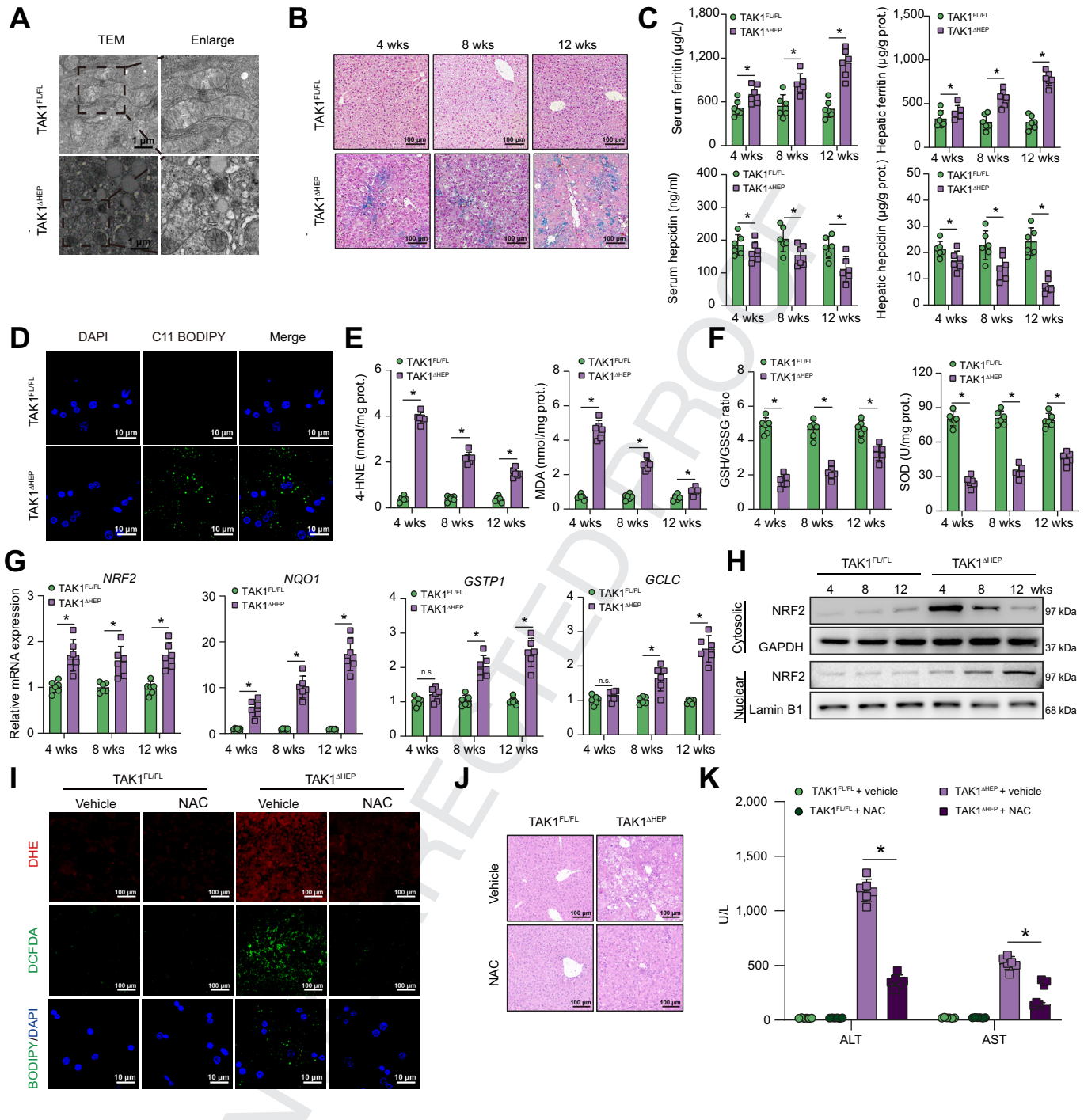

Fig. 6. TAK1 deficiency promoted ferroptosis of hepatocytes by inducing oxidative stress. (A) Representative TEM images from liver tissues (4,800 × magnification, scale bars = 1 μm, n = six per group). (B) Perls' Prussian Blue staining of liver samples at different times. (C) Serum and hepatic levels of ferritin and hepcidin. (D) Representative confocal images of primary hepatocytes labelled with C11-BODIPY and DAPI (200 × magnification, scale bars = 25 μm). (E, F) Hepatic MDA, 4-HNE, and SOD levels and GSH/GSSG ratio at different times. (G) The expression levels of gene NRF2, NQO1, GSTP1, and GCLC in liver tissue, n = 6 mice/group. (H) Western blot was performed to analyse the levels of NRF2 in cytosolic and nuclear of primary hepatocytes of TAK1$^{FL/FL}$ and TAK1$^{\Delta HEP}$ mice. TAK1$^{FL/FL}$ and TAK1$^{\Delta HEP}$ mice were treated with i.p. injections of NAC (150 mg/kg/day) or vehicle from 2 weeks of age to 4 weeks of age, (I) representative immunofluorescence staining images of DHE and DCFDA in liver sections (200 × magnification, scale bars = 100 μm) and primary hepatocytes labelled with C11-BODIPY and DAPI (200 × magnification, scale bars = 25 μm). (J) Representative H&E staining images in liver sections. (K) Serum ALT and AST levels. Data are presented as the mean ± SEM (n = 6). *p <0.05 Mann–Whitney U test. ALT, alanine aminotransferase; AST, aspartate aminotransferase; DCFDA, 2′,7′-dichlordihydrofluorescein diacetate; GAPDH, glyceraldehyde-3-phosphate dehydrogenase; GSH, glutathione; GSSG, glutathione disulfide; 4-HNE, 4-hydroxynonenal; MDA, malondialdehyde; NRF2, nuclear factor erythroid 2-related factor 2; SOD, superoxide dismutase; TAK1, transforming growth factor-beta-activated kinase 1; TEM, transmission electron microscopy; w, weeks.

FLA 5.6.0 DTD ■ JHEPR100695_proof ■ 9 March 2023 ■ 5:04 am ■ ce

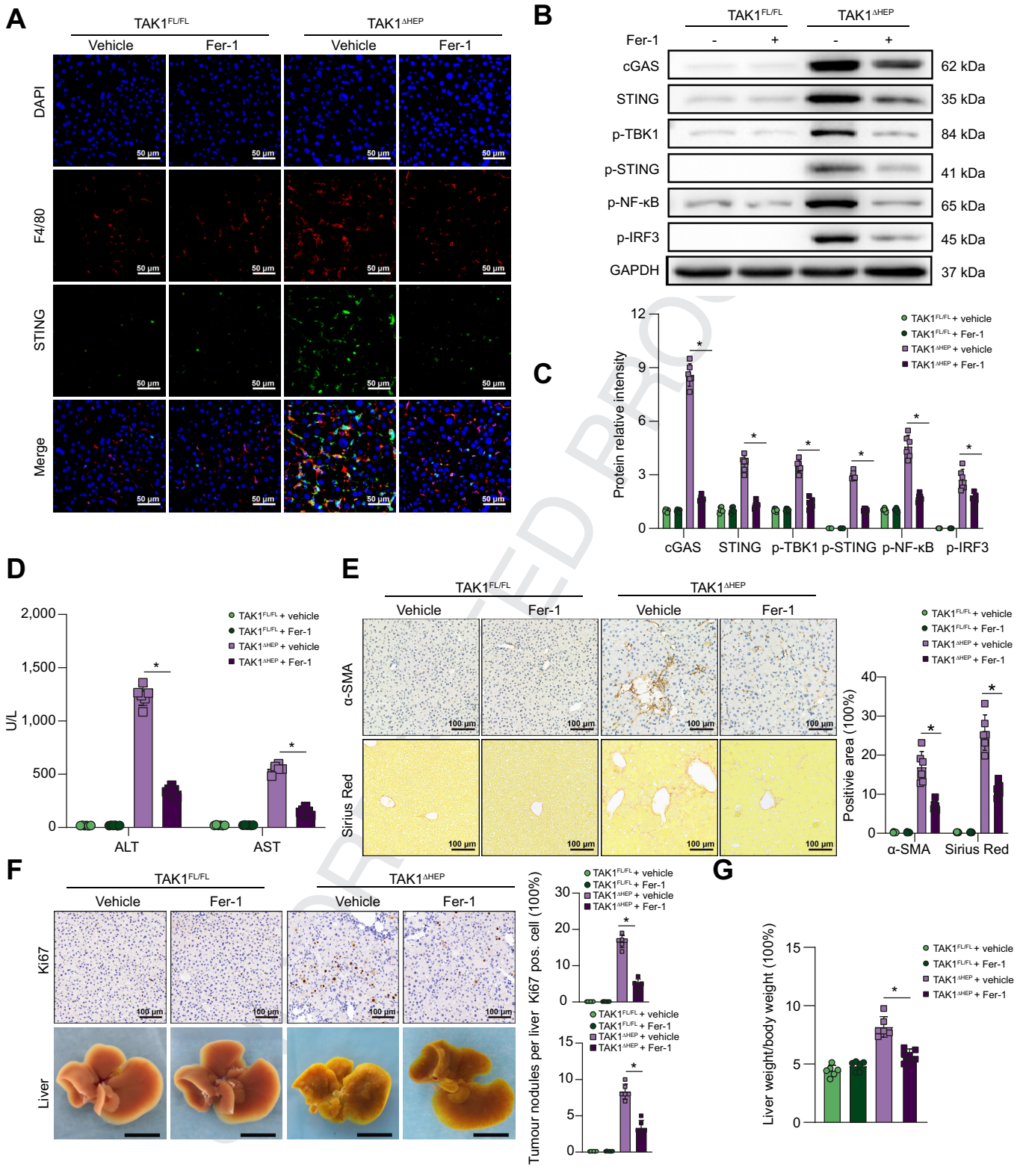

Fig. 7. Inhibition of hepatocellular ferroptosis decreased macrophage STING activation and suppressed liver injury, fibrosis, and tumorigenesis in TAK1$^{\Delta HEP}$ mice. TAK1$^{FL/FL}$ and TAK1$^{\Delta HEP}$ mice were treated with Fer-1 (5 mg/kg/day) or vehicle from 2 weeks of age. Mice were sacrificed at 4, 8, and 12 weeks of age. At 4 weeks of age, (A) representative immunofluorescence images from liver tissues stained with STING and F4/80 (400 × magnification, scale bars = 50 μm); (B, C) Western blot analysis of cGAS-STING signalling in primary macrophages; (D) Serum ALT and AST levels. At 8 weeks of age, liver sections were stained for (E) α-SMA and Sirius Red by immunohistochemistry (200 × magnification, scale bars=100 μm). At 12 weeks of age, (F) tumorigenesis was evaluated by Ki67 immunostaining in liver sections (200 × magnification, scale bars = 100 μm), tumour nodules of livers (scale bars=1 cm), and liver-to-body weight ratio (G). Data are presented as the mean ± SEM (n = 6). *p <0.05 Mann–Whitney U test. cGAS, cyclic GMP-AMP synthase; Fer-1, ferrostatin-1; GAPDH, glyceraldehyde-3-phosphate dehydrogenase; NF-κB, nuclear factor-kappa B; STING, stimulator of interferon genes; TAK1, transforming growth factor-beta-activated kinase 1.

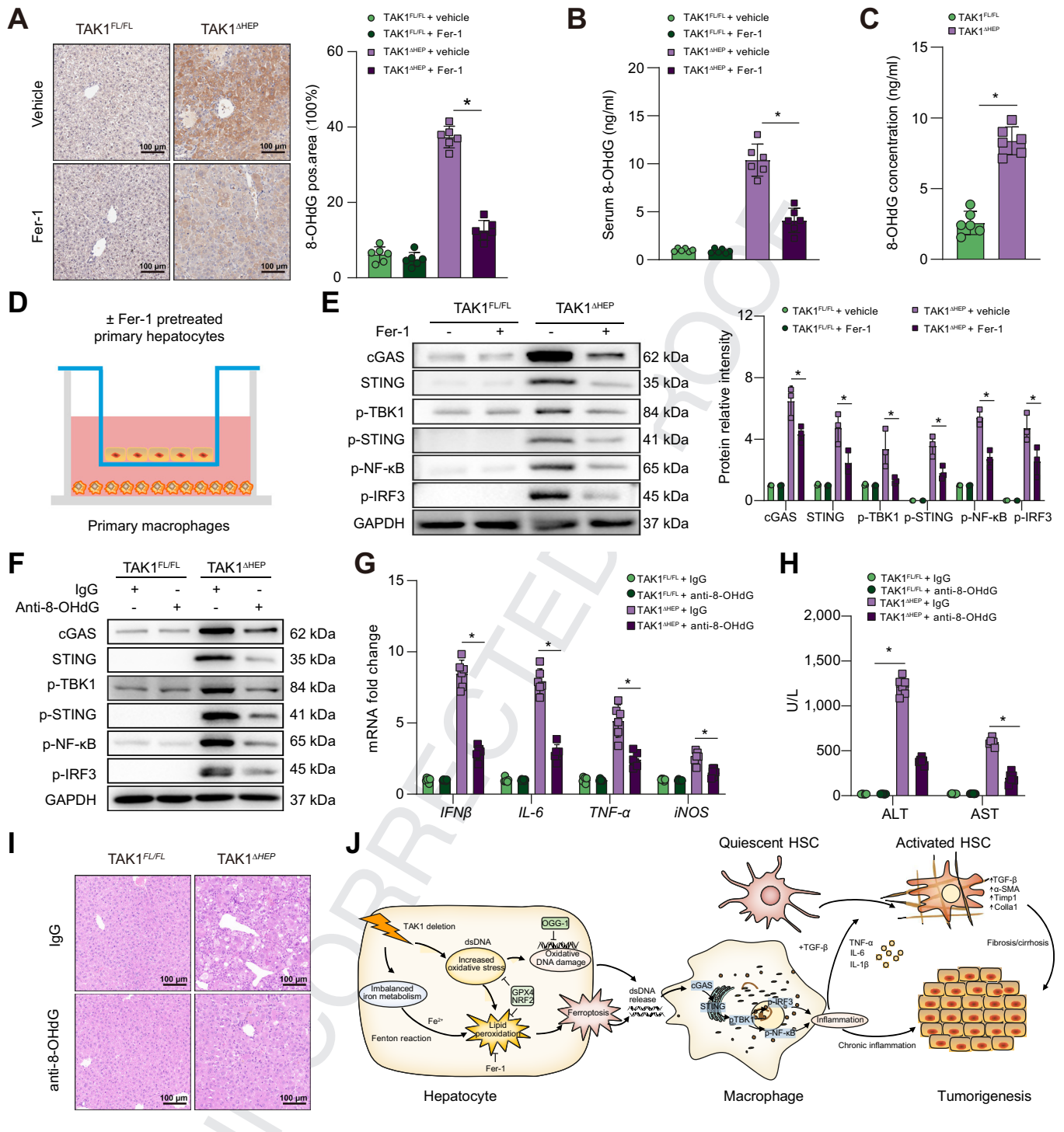

Fig. 8. Hepatocyte ferroptosis promoted oxidative DNA damage to activate macrophage cGAS-STING signalling. Mice were treated with Fer-1 (5 mg/kg/day, from 2 weeks to 4 weeks of age) or vehicle, (A) immunohistochemical detection of 8-OHdG in liver samples (200 × magnification, scale bars = 100 μm), and (B) serum levels of 8-OHdG. (C) Level of 8-OHdG in the culture media of primary hepatocytes. (D) Isolated primary hepatocytes from TAK1$^{FL/FL}$ or TAK1$^{\Delta HEP}$ mice were pretreated with or without Fer-1 (2 μM) for 6 h and then co-cultured with primary macrophages for 12 h. Primary macrophages were harvested to perform Western blots for (E) cGAS-STING signal pathway. TAK1$^{FL/FL}$ and TAK1$^{\Delta HEP}$ mice were i.p. injected with control IgG or anti-8-OHG antibody from 2 weeks to 4 weeks of age, primary liver macrophages were isolated for (F) Western blots for cGAS-STING signal pathway and (G) RT-qPCR analysis was performed for *IFN-β, IL-6, TNF-α* and *iNOS* gene expression, (H) serum ALT and AST levels, (I) representative H&E staining images in liver sections (200 × magnification, scale bars = 100 μm). (J) Schematic illustration of how TAK1 deficiency induce hepatocyte ferroptosis to promote liver tumorigenesis via macrophage cGAS-STING signalling. Data are presented as the mean ± SEM (n = 6). *p <0.05 Mann–Whitney U test. ALT, alanine aminotransferase; AST, aspartate aminotransferase; cGAS, cyclic GMP-AMP synthase; Fer-1, ferrostatin-1; HSC, hepatic stellate cells; IFN-β, interferon-beta; NRF2, nuclear factor erythroid 2-related factor 2; OGG-1, 8-oxoguanine DNA glycosylase 1; 8-OHdG, 8-hydroxydeoxyguanosine; STING, stimulator of interferon genes; TAK1, transforming growth factor-beta-activated kinase 1; TNF-α, tumour necrosis factor-alpha.

signalling during liver injury, fibrosis, and tumorigenesis remains unclear. Here, we found that TAK1 deficiency promoted hepatocellular ferroptosis, which facilitated macrophage STING activation and subsequent liver injury and inflammation. Liver injury and fibrosis were attenuated by suppression of STING activation in macrophages. Inhibition of ferroptosis suppressed liver injury, fibrosis, and hepatocarcinogenesis.

Emerging evidence suggests that TAK1 signalling plays a crucial role in human liver cancers. Increased TAK1 expression in human HCCs was associated with vascular invasion and poor overall survival.[26] Another study revealed a correlation between high TAK1 expression and low GRAMD4 expression in HCC patients. Mechanistically, GRAMD4 inhibited HCC migration, invasion, and metastasis by promoting TAK1 degradation.[25] Recent research has demonstrated the clinical relevance of TAK1 in promoting HCC and sorafenib resistance. Combining TAK1 inhibitors with sorafenib inhibited the growth of sorafenib-resistant HCCLM3 xenografts in mouse models.[41]

In contrast, numerous studies have documented spontaneous liver fibrosis and hepatocarcinogenesis in mice with hepatocyte-specific deletion of TAK1,[27,32,39,42] which seemed to contradict the findings in human liver cancers. Studies with mouse models of hepatocyte-specific TAK1 deficiency focused primarily on the role of TAK1 in regulating tumorigenesis, whereas human samples were utilised to investigate the effects of TAK1 on regulating progression, metastasis, and therapeutic response. In addition, TAK1A but not TAK1B functioned as a tumour cell migratory mediator, revealing an isoform-specific role of TAK1.[26] Taken together, TAK1 is theorised to have potential roles that differ by stage. Although TAK1 depletion can promote the initial development of chronic liver injury and tumorigenesis, TAK1 inhibition exerts a therapeutic effect in tumour treatment. Therefore, further basic and clinical research are needed to determine the precise context dependent, cell type-dependent and isoform-specific role of TAK1 signalling in regulating liver tumour initiation, progression, metastasis, and therapeutic response.

Oxidative stress is an imbalance between the production of free radicals and antioxidants and is implicated in many human diseases. Overproduction of ROS is a constant threat to cytosolic DNA, both nuclear and mitochondrial DNA; when left unrepaired, this damage also seems to be involved in mutagenicity and cancer promotion.[43] Oxidative DNA damage has been demonstrated to result in cytotoxic effects and is implicated in the pathogenesis of inflammation-associated diseases.[44] It was found that the levels of markers of lipid peroxidation and oxidative DNA damage, such as HNE and 8-OHdG, are correlated with the severity of necroinflammation and fibrosis in patients with non-alcoholic fatty liver disease.[45] Increased hepatic oxidative DNA damage was found in patients with non-alcoholic steatohepatitis who developed hepatocellular carcinoma, and 8-OHdG content in liver tissue may serve as a marker of oxidative stress and could be a particularly useful predictor of hepatocarcinogenesis.[46] Additionally, patients with high serum alpha-fetoprotein and a high degree of ballooning showed accumulation of oxidative DNA damage that could be responsible for hepatocarcinogenesis.[47]

Studies have shown the critical role of TAK1 in regulating cellular redox homeostasis. TAK1 deficiency induced increase of ROS and cell death in keratinocytes, intestinal epithelial cells, and bone marrow-derived macrophages.[48–50] In the present study, we found that TAK1 deficiency caused accumulation of ROS in hepatocytes, contributing to hepatocytes ferroptosis. Different types of cell death can cause different extents of immune and inflammatory responses. In contrast to apoptosis, ferroptosis is a form of inflammatory cell death caused by the release of DAMPs, such as HMGB1 and mtDNA, or lipid oxidation products.[3] Ferroptosis-associated inflammation plays a critical role in modulating various types of liver diseases. Inhibition of iron overload-induced ferroptosis attenuated liver injury and fibrosis.[51] Ferroptosis inhibition protected hepatocytes from necrotic death and suppressed the initial inflammatory reaction in steatohepatitis.[52] The ferroptosis inhibitor Fer-1 rescued liver fibrosis induced by either high dietary iron or carbon tetrachloride injections.[53] Ferroptosis has been implicated in the development and therapeutic responses of various types of tumours.[5] Several drugs that are already in clinical use, such as sorafenib, can induce ferroptosis in different solid tumour cells.[54] However, ferroptotic damage could also promote tumour growth by triggering inflammation-associated immunosuppression in the tumour microenvironment. $KRASG^{12D}$, a DAMP released from ferroptotic cancer cells, can be taken up by macrophages to promote M2 polarisation and subsequent pancreatic tumour growth.[55]

Increasing evidence has shown the interplay between ferroptosis and STING signalling.[56] DAMPs released from ferroptotic cells activated cGAS-STING signalling. Ferroptosis promoted 8-OHG release and thus activated the STING-dependent DNA sensor pathway to promote pancreatic tumorigenesis.[57] Another study also found that DNA damage-induced STING activation promoted autophagy-dependent ferroptosis in human pancreatic cancer cells.[58] STING activation produces excessive lipid peroxidation, leading to macrophage cell death during intestinal ischemic injury.[59] In the present study, macrophage STING was continuously activated, although its degree of activation gradually decreased at the late stage of liver fibrosis and tumour development. Interfering with STING signalling pathway has shown promise in the treatment of inflammatory, autoimmune, and cancerous diseases.[60] STING inhibitors were developed by inhibiting the binding of cGAMP to STING or the post-translational modification of STING.[61] Currently, several STING antagonist programs are undergoing pre-clinical research and the drug discovery procedure, but none have yet reached the clinical evaluation stage.[8,62,63] There are still many challenges that need to be overcome to fully realise the therapeutic potential of targeting the STING pathway, such as, patient heterogeneity, specificity, and efficacy of the inhibitors, and the complex interactions between the STING signalling pathway and other cellular pathways. Accumulating evidence indicates that ferroptosis and STING interact in both human diseases and mouse models. In patients with colon cancer, STING-related genes were interrelated with ferroptosis at the levels of genes and proteins.[64] Ferroptosis promoted 8-OHG release and thus activated the STING-dependent DNA sensor pathway to promote pancreatic tumorigenesis.[57] The inhibition of ferroptosis ameliorated acute liver damage by inhibiting STING activation.[65] However, STING signalling plays a crucial role in numerous forms of cell death, including ferroptosis.[66,67] Moreover, co-immunoprecipitation studies demonstrated that STING could interact with the TAK1 protein, indicating an interaction between STING and TAK1.[68] However, the relationship between STING expression and TAK1 expression in human diseases remains unclear.

In conclusion, these findings reveal the critical interplay between hepatocyte ferroptosis and macrophage STING activation. Hepatocellular ferroptosis promotes the activation of

macrophage STING signalling, which in turn facilitates the development of spontaneous liver injury, fibrosis, and hepatocellular carcinoma. Our study uncovered a novel mechanism of STING activation and suggests a new approach for modulating ferroptosis- and STING-dependent immunopathologies. Strategies targeting macrophage STING signalling or hepatocellular ferroptosis could be beneficial in the treatment of liver injury, fibrosis, and tumours.

Abbreviations

ALI, acute liver injury; ALT, alanine aminotransferase; AST, aspartate aminotransferase; cGAS, cyclic GMP-AMP synthase; CM, conditioned media; DAMPs, damage-associated molecular patterns; DCFDA, 2′,7′-dichlorodihydrofluorescein diacetate; DHE, dihydroethidium; Fer-1, ferrostatin-1; GAPDH, glyceraldehyde-3-phosphate dehydrogenase; GEO, Gene Expression Omnibus; GSH, glutathione; GSSG, glutathione disulfide; HCC, hepatocellular carcinoma; 4-HNE, 4-hydroxynonenal; HSCs, hepatic stellate cells; IFN-β, interferon-beta; MAP3K, MAP kinase kinase kinase; MDA, malondialdehyde; NF-κB, nuclear factor-kappa B; NK, natural killer; NPC, nonparenchymal cell; NRF2, nuclear factor erythroid 2-related factor 2; OGG1, 8-oxoguanine DNA glycosylase 1; 8-OHdG, 8-hydroxydeoxyguanosine; PCD, programmed cell death; ROS, reactive oxygen species; SOD, superoxide dismutase; STING, stimulator of interferon genes; TGF-β, transforming growth factor-beta; TAK1, transforming growth factor-beta-activated kinase 1; TNF-α, tumour necrosis factor-alpha.

Financial support

This study was supported by grants from the National Natural Science Foundation of China (82071798, 81971495) and the CAMS Innovation Fund for Medical Sciences (No. 2019-I2M-5-035).

Conflicts of interest

The authors declare that they have no conflicts of interest.

Please refer to the accompanying ICMJE disclosure forms for further details.

Authors' contributions

Drafted the manuscript: WS, WG. Conducted the experiments and analysed the data: WS, WG, RZ, QW, L. Li, QB, ZX, ZL, MW. Participated in the research design: WS, WG, HZ, XW, L. Lu. Revised the manuscript: YZ, GW, HZ, XW. All authors discussed the results and contributed to the final manuscript.

Data availability statement

Data are available on reasonable request to the corresponding author.

Supplementary data

Supplementary data to this article can be found online at https://doi.org/10.1016/j.jhepr.2023.100695.

References

Author names in bold designate shared co-first authorship

[1] Jiang X, Stockwell BR, Conrad M. Ferroptosis: mechanisms, biology and role in disease. Nat Rev Mol Cel Biol 2021;22:266–282.
[2] **Wu Y**, **Zhang S**, **Gong X**, Tam S, Xiao D, Liu S, et al. The epigenetic regulators and metabolic changes in ferroptosis-associated cancer progression. Mol Cancer 2020;19:39.
[3] Tang D, Chen X, Kang R, Kroemer G. Ferroptosis: molecular mechanisms and health implications. Cell Res 2021;31:107–125.
[4] Chen X, Zeh HJ, Kang R, Kroemer G, Tang D. Cell death in pancreatic cancer: from pathogenesis to therapy. Nat Rev Gastroenterol Hepatol 2021;18:804–823.
[5] Chen X, Kang R, Kroemer G, Tang D. Broadening horizons: the role of ferroptosis in cancer. Nat Rev Clin Oncol 2021;18:280–296.
[6] Nathan C, Cunningham-Bussel A. Beyond oxidative stress: an immunologist's guide to reactive oxygen species. Nat Rev Immunol 2013;13:349–361.
[7] **Liang D**, **Minikes AM**, **Jiang X**. Ferroptosis at the intersection of lipid metabolism and cellular signaling. Mol Cel 2022;82:2215–2227.
[8] Decout A, Katz JD, Venkatraman S, Ablasser A. The cGAS-STING pathway as a therapeutic target in inflammatory diseases. Nat Rev Immunol 2021;21:548–569.
[9] Kwon J, Bakhoum SF. The cytosolic DNA-sensing cGAS-STING pathway in cancer. Cancer Discov 2020;10:26–39.
[10] Marcus A, Mao AJ, Lensink-Vasan M, Wang L, Vance RE, Raulet DH. Tumor-Derived cGAMP triggers a STING-mediated interferon response in non-tumor cells to activate the NK cell response. Immunity 2018;49:754–763.e4.
[11] Barbie DA, Tamayo P, Boehm JS, Kim SY, Moody SE, Dunn IF, et al. Systematic RNA interference reveals that oncogenic KRAS-driven cancers require TBK1. Nature 2009;462:108–112.
[12] Li T, Chen ZJ. The cGAS-cGAMP-STING pathway connects DNA damage to inflammation, senescence, and cancer. J Exp Med 2018;215:1287–1299.
[13] Ahmed O, Robinson MW, O'Farrelly C. Inflammatory processes in the liver: divergent roles in homeostasis and pathology. Cell Mol Immunol 2021;18:1375–1386.
[14] Aggarwal BB, Vijayalekshmi RV, Sung B. Targeting inflammatory pathways for prevention and therapy of cancer: short-term friend, long-term foe. Clin Cancer Res 2009;15:425–430.
[15] Shim JH, Xiao C, Paschal AE, Bailey ST, Rao P, Hayden MS, et al. TAK1, but not TAB1 or TAB2, plays an essential role in multiple signaling pathways in vivo. Genes Dev 2005;19:2668–2681.
[16] Liu W, Chang BL, Cramer S, Koty PP, Li T, Sun J, et al. Deletion of a small consensus region at 6q15, including the MAP3K7 gene, is significantly associated with high-grade prostate cancers. Clin Cancer Res 2007;13:5028–5033.
[17] Lamothe B, Lai Y, Hur L, Orozco NM, Wang J, Campos AD, et al. Deletion of TAK1 in the myeloid lineage results in the spontaneous development of myelomonocytic leukemia in mice. PLoS One 2012;7:e51228.
[18] Wu M, Shi L, Cimic A, Romero L, Sui G, Lees CJ, et al. Suppression of Tak1 promotes prostate tumorigenesis. Cancer Res 2012;72:2833–2843.
[19] Roh YS, Song J, Seki E. TAK1 regulates hepatic cell survival and carcinogenesis. J Gastroenterol 2014;49:185–194.
[20] Cordas Dos Santos DM, Eilers J, Sosa Vizcaino A, Orlova E, Zimmermann M, Stanulla M, et al. MAP3K7 is recurrently deleted in pediatric T-lymphoblastic leukemia and affects cell proliferation independently of NF-kappaB. BMC Cancer 2018;18:663.
[21] **Wen J**, **Hu Y**, **Luo KJ**, Yang H, Zhang SS, Fu JH. Positive transforming growth factor-beta activated kinase-1 expression has an unfavorable impact on survival in T3N1-3M0 esophageal squamous cell carcinomas. Ann Thorac Surg 2013;95:285–290.
[22] Lin P, Niu W, Peng C, Zhang Z, Niu J. The role of TAK1 expression in thyroid cancer. Int J Clin Exp Pathol 2015;8:14449–14456.
[23] Yang Y, Qiu Y, Tang M, Wu Z, Hu W, Chen C. Expression and function of transforming growth factor-beta-activated protein kinase 1 in gastric cancer. Mol Med Rep 2017;16:3103–3110.
[24] Zhao P, Wang S, Jiang J, Liu H, Zhu X, Zhao N, et al. TIPE2 sensitizes osteosarcoma cells to cis-platin by down-regulating MDR1 via the TAK1- NF-kappaB and - AP-1 pathways. Mol Immunol 2018;101:471–478.
[25] **Ge QY**, **Chen J**, **Li GX**, Tan XL, Song J, Ning D, et al. GRAMD4 inhibits tumour metastasis by recruiting the E3 ligase ITCH to target TAK1 for degradation in hepatocellular carcinoma. Clin Transl Med 2021;11:e635.
[26] Ridder DA, Urbansky LL, Witzel HR, Schindeldecker M, Weinmann A, Berndt K, et al. Transforming growth factor-beta activated kinase 1 (Tak1) is activated in hepatocellular carcinoma, mediates tumor progression, and predicts unfavorable outcome. Cancers (Basel) 2022;14:430.
[27] Inokuchi-Shimizu S, Park EJ, Roh YS, Yang L, Zhang B, Song J, et al. TAK1-mediated autophagy and fatty acid oxidation prevent hepatosteatosis and tumorigenesis. J Clin Invest 2014;124:3566–3578.
[28] **Malireddi RKS**, **Gurung P**, Kesavardhana S, Samir P, Burton A, Mummareddy H, et al. Innate immune priming in the absence of TAK1 drives RIPK1 kinase activity-independent pyroptosis, apoptosis, necroptosis, and inflammatory disease. J Exp Med 2020:217. https://doi.org/10.1084/jem.20191644.

[29] Orning P, **Weng D**, **Starheim K**, **Ratner D**, Best Z, Lee B, et al. Pathogen blockade of TAK1 triggers caspase-8-dependent cleavage of gasdermin D and cell death. Science 2018;362:1064–1069.
[30] Zhou N, Bao J. FerrDb: a manually curated resource for regulators and markers of ferroptosis and ferroptosis-disease associations. Database (Oxfofd) 2020:2020. https://doi.org/10.1093/database/baaa021.
[31] **DeTomaso D**, **Jones MG**, Subramaniam M, Ashuach T, Ye CJ, Yosef N. Functional interpretation of single cell similarity maps. Nat Commun 2019;10:4376.
[32] Inokuchi S, Aoyama T, Miura K, Osterreicher CH, Kodama Y, Miyai K, et al. Disruption of TAK1 in hepatocytes causes hepatic injury, inflammation, fibrosis, and carcinogenesis. Proc Natl Acad Sci U S A 2010;107:844–849.
[33] **Chen C**, **Yang RX**, Xu HG. STING and liver disease. J Gastroenterol 2021;56:704–712.
[34] Mao Y, Luo W, Zhang L, Wu W, Yuan L, Xu H, et al. STING-IRF3 triggers endothelial inflammation in response to free fatty acid-induced mitochondrial damage in diet-induced obesity. Arterioscler Thromb Vasc Biol 2017;37:920–929.
[35] **Domizio JD**, **Gulen MF**, **Saidoune F**, **Thacker VV**, **Yatim A**, Sharma K, et al. The cGAS-STING pathway drives type I IFN immunopathology in COVID-19. Nature 2022;603:145–151.
[36] Hopfner KP, Hornung V. Molecular mechanisms and cellular functions of cGAS-STING signalling. Nat Rev Mol Cel Biol 2020;21:501–521.
[37] Zhong W, Rao Z, Rao J, Han G, Wang P, Jiang T, et al. Aging aggravated liver ischemia and reperfusion injury by promoting STING-mediated NLRP3 activation in macrophages. Aging Cell 2020;19:e13186.
[38] **Wang Q**, **Zhou H**, **Bu Q**, Wei S, Li L, Zhou J, et al. Role of XBP1 in regulating the progression of non-alcoholic steatohepatitis. J Hepatol 2022;77:312–325.
[39] Tan S, Zhao J, Sun Z, Cao S, Niu K, Zhong Y, et al. Hepatocyte-specific TAK1 deficiency drives RIPK1 kinase-dependent inflammation to promote liver fibrosis and hepatocellular carcinoma. Proc Natl Acad Sci U S A 2020;117:14231–14242.
[40] Luedde T, Kaplowitz N, Schwabe RF. Cell death and cell death responses in liver disease: mechanisms and clinical relevance. Gastroenterology 2014;147:765–783.e4.
[41] Xia S, Ji L, Tao L, Pan Y, Lin Z, Wan Z, et al. TAK1 is a novel target in hepatocellular carcinoma and contributes to sorafenib resistance. Cell Mol Gastroenterol Hepatol 2021;12:1121–1143.
[42] Yang L, Inokuchi S, Roh YS, Song J, Loomba R, Park EJ, et al. Transforming growth factor-beta signaling in hepatocytes promotes hepatic fibrosis and carcinogenesis in mice with hepatocyte-specific deletion of TAK1. Gastroenterology 2013;144:1042–1054.e4.
[43] Mao P, Wyrick JJ. Organization of DNA damage, excision repair, and mutagenesis in chromatin: a genomic perspective. DNA Repair (Amst) 2019;81:102645.
[44] Kawanishi S, Ohnishi S, Ma N, Hiraku Y, Murata M. Crosstalk between DNA damage and inflammation in the multiple steps of carcinogenesis. Int J Mol Sci 2017;18:1808.
[45] Takaki A, Kawai D, Yamamoto K. Multiple hits, including oxidative stress, as pathogenesis and treatment target in non-alcoholic steatohepatitis (NASH). Int J Mol Sci 2013;14:20704–20728.
[46] Tanaka S, Miyanishi K, Kobune M, Kawano Y, Hoki T, Kubo T, et al. Increased hepatic oxidative DNA damage in patients with nonalcoholic steatohepatitis who develop hepatocellular carcinoma. J Gastroenterol 2013;48:1249–1258.
[47] Nishida N, Yada N, Hagiwara S, Sakurai T, Kitano M, Kudo M. Unique features associated with hepatic oxidative DNA damage and DNA methylation in non-alcoholic fatty liver disease. J Gastroenterol Hepatol 2016;31:1646–1653.
[48] Omori E, Morioka S, Matsumoto K, Ninomiya-Tsuji J. TAK1 regulates reactive oxygen species and cell death in keratinocytes, which is essential for skin integrity. J Biol Chem 2008;283:26161–26168.
[49] Kajino-Sakamoto R, Omori E, Nighot PK, Blikslager AT, Matsumoto K, Ninomiya-Tsuji J. TGF-beta-activated kinase 1 signaling maintains intestinal integrity by preventing accumulation of reactive oxygen species in the intestinal epithelium. J Immunol 2010;185:4729–4737.
[50] Lopez-Perez W, Sai K, Sakamachi Y, Parsons C, Kathariou S, Ninomiya-Tsuji J. TAK1 inhibition elicits mitochondrial ROS to block intracellular bacterial colonization. Proc Natl Acad Sci U S A 2021;118:e2023647118.
[51] **Wu A**, **Feng B**, **Yu J**, **Yan L**, Che L, Zhuo Y, et al. Fibroblast growth factor 21 attenuates iron overload-induced liver injury and fibrosis by inhibiting ferroptosis. Redox Biol 2021;46:102131.
[52] Tsurusaki S, Tsuchiya Y, Koumura T, Nakasone M, Sakamoto T, Matsuoka M, et al. Hepatic ferroptosis plays an important role as the trigger for initiating inflammation in nonalcoholic steatohepatitis. Cell Death Dis 2019;10:449.
[53] **Yu Y**, **Jiang L**, Wang H, Shen Z, Cheng Q, Zhang P, et al. Hepatic transferrin plays a role in systemic iron homeostasis and liver ferroptosis. Blood 2020;136:726–739.
[54] Lachaier E, Louandre C, Godin C, Saidak Z, Baert M, Diouf M, et al. Sorafenib induces ferroptosis in human cancer cell lines originating from different solid tumors. Anticancer Res 2014;34:6417–6422.
[55] Dai E, Han L, Liu J, Xie Y, Kroemer G, Klionsky DJ, et al. Autophagy-dependent ferroptosis drives tumor-associated macrophage polarization via release and uptake of oncogenic KRAS protein. Autophagy 2020;16:2069–2083.
[56] Zhang R, Kang R, Tang D. The STING1 network regulates autophagy and cell death. Signal Transduct Target Ther 2021;6:208.
[57] Dai E, Han L, Liu J, Xie Y, Zeh HJ, Kang R, et al. Ferroptotic damage promotes pancreatic tumorigenesis through a TMEM173/STING-dependent DNA sensor pathway. Nat Commun 2020;11:6339.
[58] Kuang F, Liu J, Li C, Kang R, Tang D. Cathepsin B is a mediator of organelle-specific initiation of ferroptosis. Biochem Biophys Res Commun 2020;533:1464–1469.
[59] **Wu J**, **Liu Q**, Zhang X, Wu X, Zhao Y, Ren J. STING-dependent induction of lipid peroxidation mediates intestinal ischemia-reperfusion injury. Free Radic Biol Med 2021;163:135–140.
[60] Guerini D. STING agonists/antagonists: their potential as therapeutics and future developments. Cells 2022;11:1159.
[61] Feng X, Liu D, Li Z, Bian J. Bioactive modulators targeting STING adaptor in cGAS-STING pathway. Drug Discov Today 2020;25:230–237.
[62] Sheridan C. Drug developers switch gears to inhibit STING. Nat Biotechnol 2019;37:199–201.
[63] Ding C, Song Z, Shen A, Chen T, Zhang A. Small molecules targeting the innate immune cGAS–STING–TBK1 signaling pathway. Acta Pharm Sin B 2020;10:2272–2298.
[64] Nie J, Shan D, Li S, Zhang S, Zi X, Xing F, et al. A novel ferroptosis related gene signature for prognosis prediction in patients with colon cancer. Front Oncol 2021;11:654076.
[65] Li Y, Yu P, Fu W, Wang S, Zhao W, Ma Y, et al. Ginsenoside Rd inhibited ferroptosis to alleviate CCl(4)-induced acute liver injury in mice via cGAS/STING pathway. Am J Chin Med 2022;28:1–15.
[66] Li C, Liu J, Hou W, Kang R, Tang D. STING1 promotes ferroptosis through MFN1/2-dependent mitochondrial fusion. Front Cel Dev Biol 2021;9:698679.
[67] **Hu X**, **Zhang H**, Zhang Q, Yao X, Ni W, Zhou K. Emerging role of STING signalling in CNS injury: inflammation, autophagy, necroptosis, ferroptosis and pyroptosis. J Neuroinflammation 2022;19:242.
[68] De Falco F, Cutarelli A, Catoi AF, Uberti BD, Cuccaro B, Roperto S. Bovine delta papillomavirus E5 oncoprotein negatively regulates the cGAS-STING signaling pathway in cattle in a spontaneous model of viral disease. Front Immunol 2022;13:937736.

Journal of Hepatology, Volume ■

Supplemental information

TAK1 deficiency promotes liver injury and tumorigenesis via ferroptosis and macrophage cGAS-STING signalling

Wantong Su, Weicheng Gao, Rui Zhang, Qi Wang, Lei Li, Qingfa Bu, Zibo Xu, Zheng Liu, Mingming Wang, Yaqing Zhu, Guoping Wu, Haoming Zhou, Xun Wang, and Ling Lu

TAK1 deficiency promotes liver injury and tumorigenesis via ferroptosis and macrophage cGAS-STING signalling

Wantong Su, Weicheng Gao, Rui Zhang, Qi Wang, Lei Li, Qingfa Bu, Zibo Xu, Zheng Liu, Mingming Wang, Yaqing Zhu, Guoping Wu, Haoming Zhou, Xun Wang, Ling Lu

Table of contents

Supplementary materials and methods

Animal treatment

Mice were maintained on either an iron-rich diet containing 2% carbonyl iron (Harlan, 2018S) or a standard diet starting at 3 weeks of age. Serum and liver samples were collected at 8 weeks of age.

Cell Isolation and Treatment

Primary mouse HSCs were isolated according to the previous study[1]. In brief, livers were perfused in situ via the portal vein with 50 ml warmed (37 °C) Hanks' balanced salt solution (Ca^{2+} and Mg^{2+} free) containing EGTA (0.5 M), followed by collagenase IV (Sigma, Saint Louis, MO, USA, 0.05% w/v, dissolved in HBSS with Ca^{2+} and Mg^{2+}). Perfused livers were dissected and teased through 70-mm nylon mesh cell strainers and centrifuged at 50 g for 3 min. The supernatant was further centrifuged at 500 g for 10 min, resuspended in Ficoll plus Percoll (1:10, GE Healthcare), and centrifuged at 1400 g for 17 min. HSCs were collected from the interface. Primary mouse HSCs were incubated with primary macrophage conditioned media (CM) for 24h.

Macrophage Polarization

To study the effects of STING inhibitors on macrophage polarization, primary liver macrophages were pretreated for 1 hour with C-176 (0.5 μM) or vehicle and then co-cultured with primary hepatocytes for 6 hours. Primary macrophages were collected for Western blot analysis and RT–qPCR.

Cell Viability Assay

Primary hepatocytes were cultured in 96-well plate, cell viability was determined using a Cell Counting Kit-8 (CCK-8) (cat# CK04, Dojindo, Japan) assay according with the manufacturer's instructions. Cells in each well were incubated with 10 μl of CCK-8 reagent. Absorbance was measured at 450 nm at different time point.

LDH Release Assay

LDH concentration of culture media was measured using the LDH Cytotoxicity Assay Kit following according with the manufacturer's instructions (cat# C0016, Beyotime, China).

Fig.S1

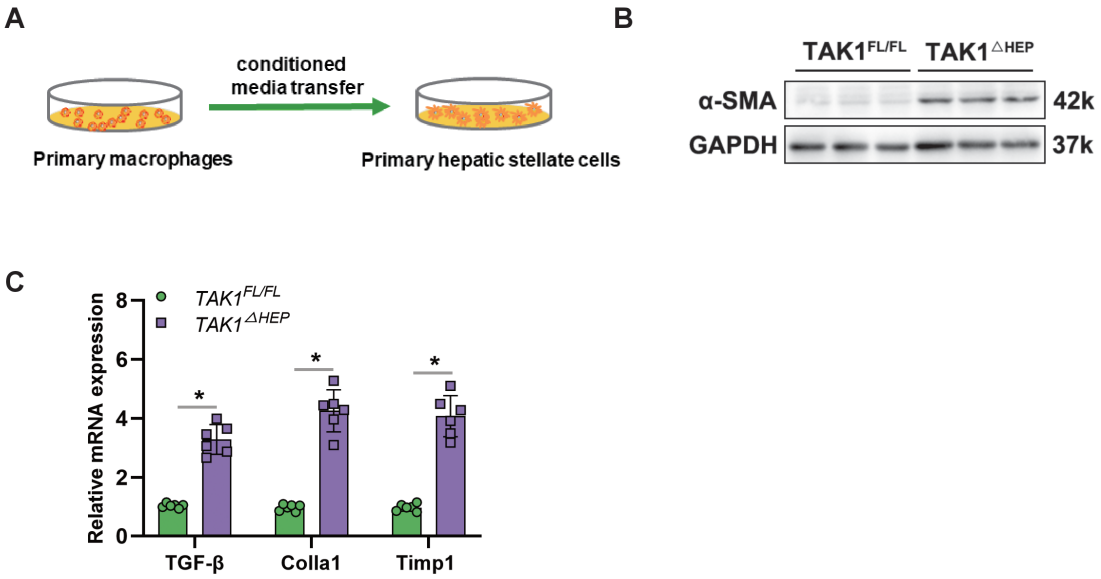

Fig.S1 Macrophages from TAK1$^{\triangle HEP}$ mice liver contributed hepatic stellate cells' activation

(A) Conditioned media of primary liver macrophage from TAK1$^{FL/FL}$ and TAK1$^{\triangle HEP}$ mice was transferred to primary hepatic stellate cells of wildtype mice for 24 hours in the presence of TGF-β1 (8 ng/mL). **(B)** α-SMA protein expression of primary HSCs. **(C)** The mRNA levels of TGF-β, Colla1, and Timp1 of primary HSCs. Data are presented as the mean ± SEM (n = 6). *$p < 0.05$ Mann–Whitney U test.

Fig. S2

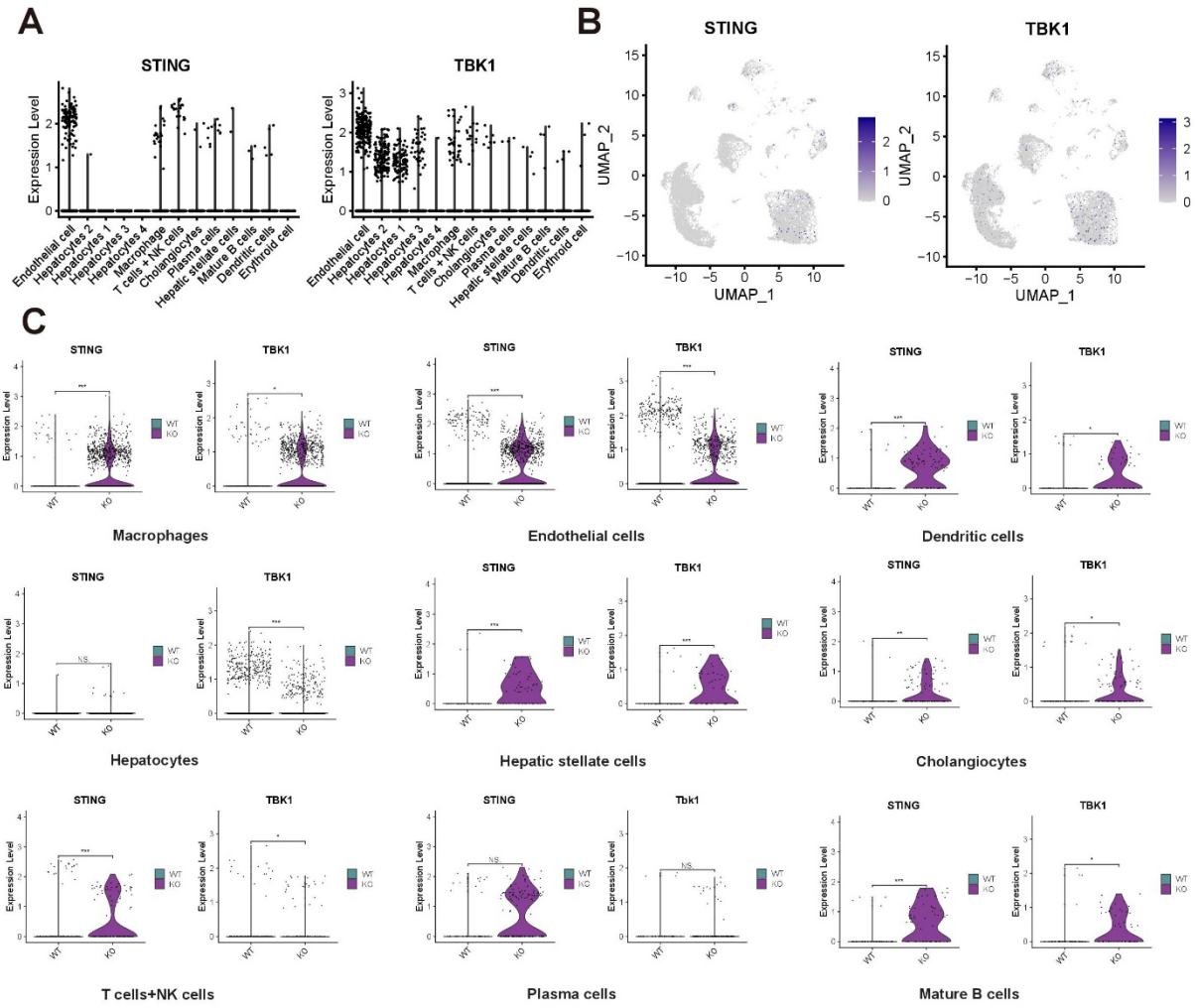

Fig. S2. STING signaling pathway related genes expression

Gene expression of all clusters were constructed using the Seurat VlnPlot & Featureplot function. Violin plots (A) and Featureplot (B) show STING and TBK1 expression across all clusters of TAK1$^{FL/FL}$ mice. (C) Violin plots of STING and TBK1 expression in macrophages of TAK1$^{FL/FL}$ and TAK1$^{\Delta HEP}$ mice. ns, not significant; * $p < 0.05$, ** $p < 0.01$, **** $p < 0.001$, Wilcoxon rank sum test. WT: TAK1$^{FL/FL}$, KO: TAK1$^{\Delta HEP}$

Fig. S3

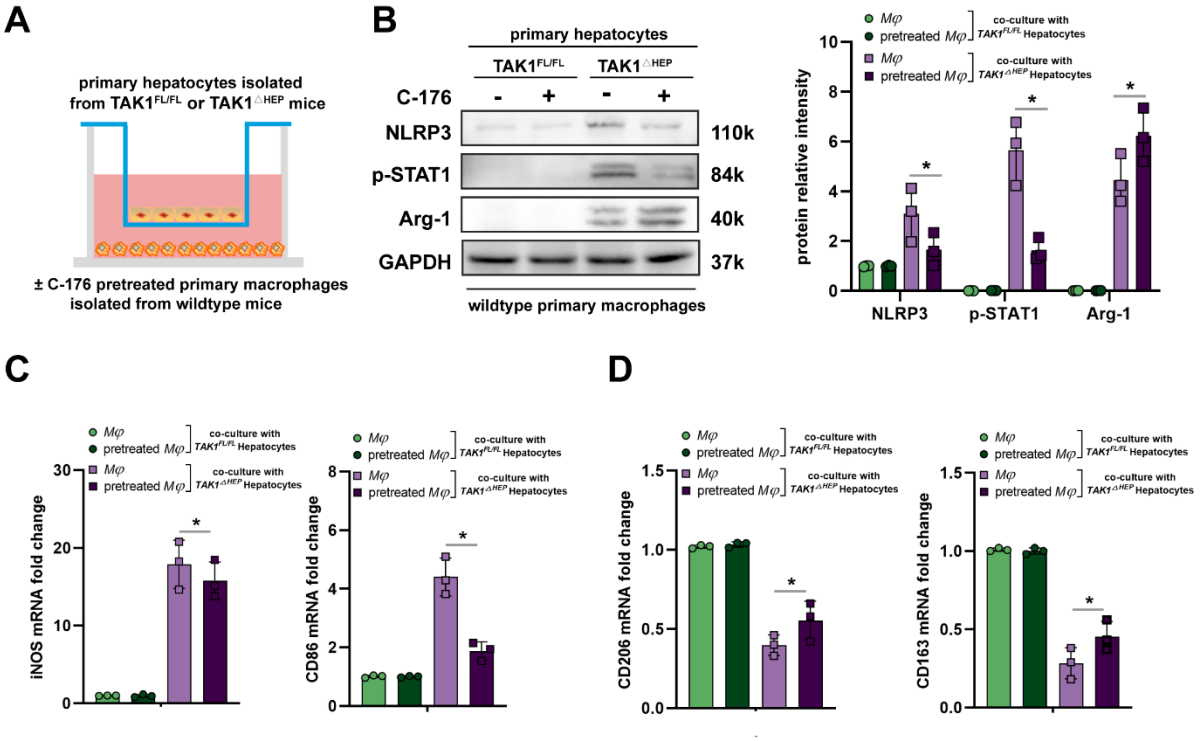

Fig. S3. C-176 impact on primary macrophage polarization.

(**A**) After pretreatment for 1 h with C-176 (0.5 μM) or vehicle, primary liver macrophages of wild-type mice were co-cultured with TAK1$^{FL/FL}$ and TAK1$^{\Delta HEP}$ primary hepatocytes for 6 h, Primary macrophages were harvested for western blots for **(B)** NLRP3**,** p-STAT1 and Arg-1, and **(C, D)** RT–qPCR analysis for iNOS, CD86, CD206 and CD163. Data are presented as the mean ± SEM (n = 3). * $p < 0.05$ Mann–Whitney U test. Mφ: primary liver macrophage

Fig. S4

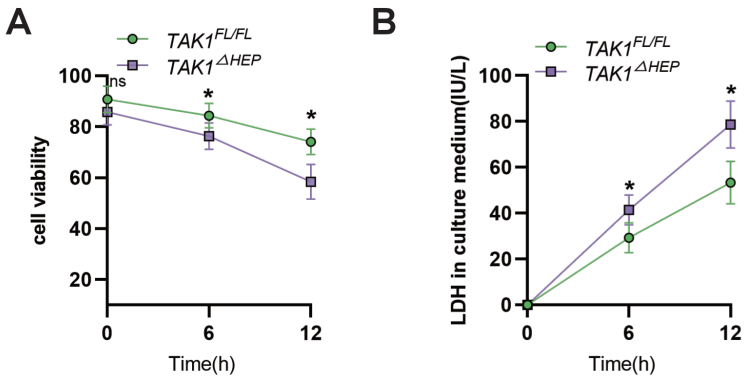

Fig.S4 Primary hepatocytes viability decreased after TAK1 deficiency.

(A) Cell viability of primary hepatocytes from $TAK1^{FL/FL}$ and $TAK1^{\triangle HEP}$ mice. **(B)** LDH level of culture media from primary hepatocytes. Data are presented as the mean ± SEM (n = 6). ns, not significant, *$p < 0.05$ Mann–Whitney U test.

Fig.S5

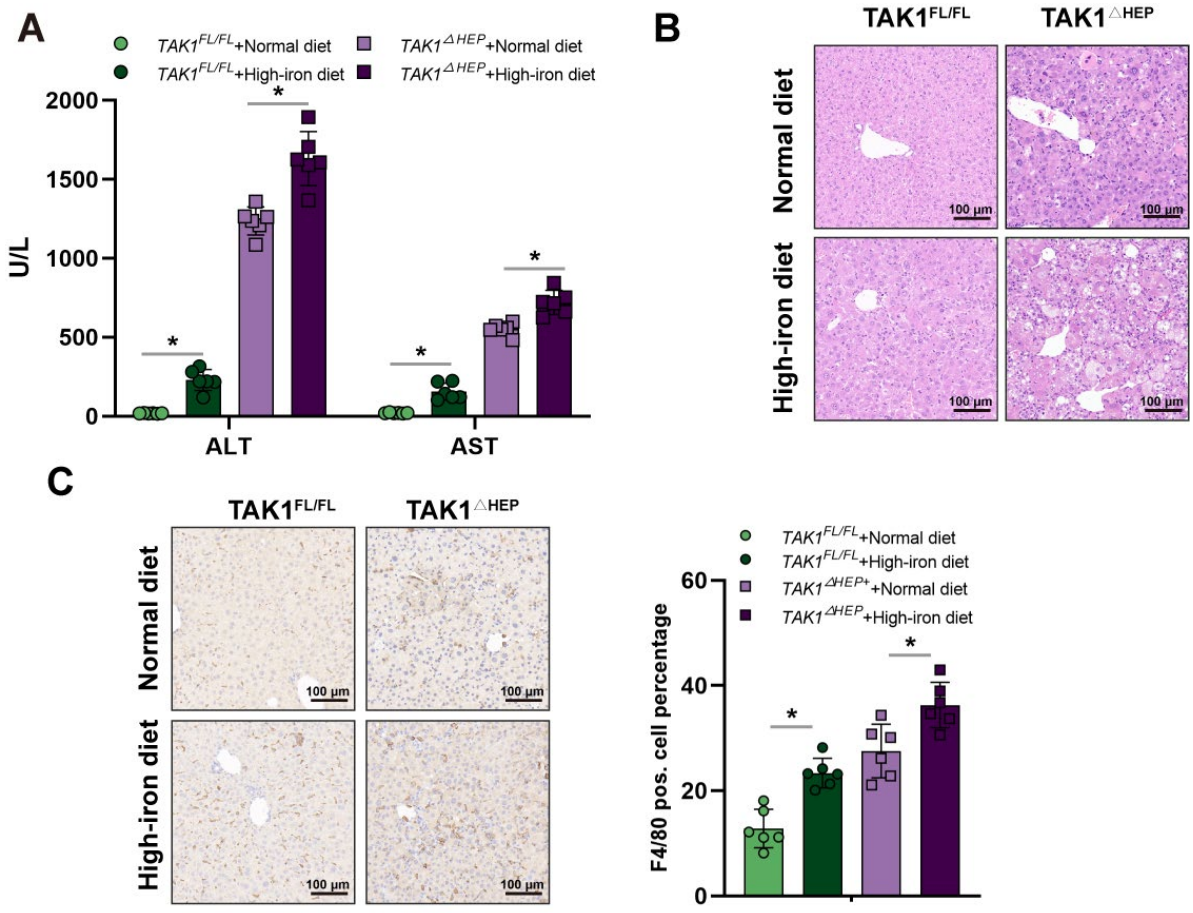

Fig.S5 High-iron diet increased liver injury and inflammation of TAK1 deficiency mice

(**A**)Serum ALT and AST levels of TAK1$^{FL/FL}$ and TAK1$^{\triangle HEP}$ mice fed with control or iron-rich diet; Data are presented as the mean ± SEM (n = 6). *$p < 0.05$ Mann–Whitney U test. (**B**) H&E and (**C**) F4/80 staining were carried out on the liver tissues of 8 weeks old TAK1$^{FL/FL}$ and TAK1$^{\triangle HEP}$ mice treated with control or iron-rich diet.

Fig. S6

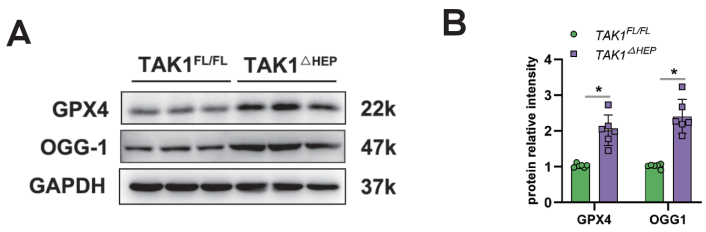

Fig.S6 Compensatory antioxidant response in TAK1 deficiency mice.

(A) Western blotting of GPX4 and OGG1 protein of TAK1FL/FL and TAK1△HEP mice liver.

(B) Quantification of GPX4 and OGG1 expression. Data are presented as the mean ± SEM (n = 6). *$p < 0.05$ Mann–Whitney U test.

Fig. S7

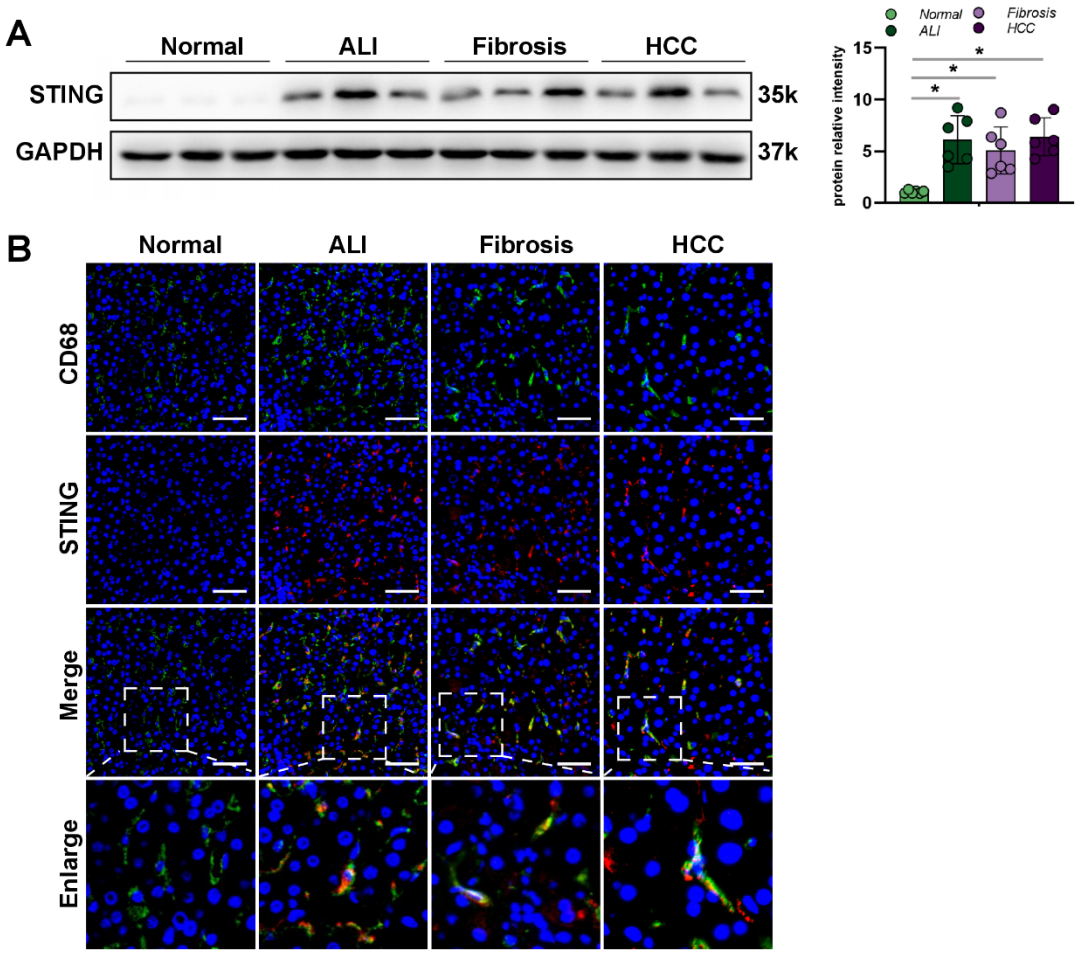

Fig. S7. Macrophage STING expression in patients with ALI, fibrosis, and HCC

Liver tissues were collected from different patients as described in Materials and Methods. (A) Western blot analysis of STING expression; Data are presented as the mean ± SEM (n = 6). * $p < 0.05$ Mann–Whitney U test. (B) Representative IF images of CD68 and STING staining (200× magnification, scale bars=100 μm).

Table S1: Sequence of primers used for RT-PCR studies

Gene	Forward Primer (5'-3')	Reverse Primer (5'-3')
GAPDH	AGGTCGGTGTGAACGGATTTG	TGTAGACCATGTAGTTGAGGTCA
CD86	GGTGGCCTTTTTGACACTCTC	TGAGGTAGAGGTAGGAGGATCTT
iNOS	GTTCTCAGCCCAACAATACAAGA	GTGGACGGGTCGATGTCAC
CD163	ATGGGTGGACACAGAATGGTT	CAGGAGCGTTAGTGACAGCAG
CD206	CTCTGTTCAGCTATTGGACGC	CGGAATTTCTGGGATTCAGCTTC
IFNβ	CCTGGAGCAGCTGAATGGAA	TGGATGGCAAAGGCAGTGTAA
TNF-α	CCCTCACACTCAGATCATCTTCT	GCTACGACGTGGGCTACAG
IL-6	TAGTCCTTCCTACCCCAATTTCC	TTGGTCCTTAGCCACTCCTTC
IL-1β	GCAACTGTTCCTGAACTCAACT	ATCTTTTGGGGTCCGTCAACT
IL-10	ACAGGGAAGAAATCGATGACA	TGGGGGAGAACCTGAAGAC
NF-κB	ATGGCAGACGATGATCCCTAC	TGTTGACAGTGGTATTTCTGGTG
TIMP1	AGGTGGTCTCGTTGATTTCT	GTAAGGCCTGTAGCTGTGCC
Col1a1	TAGGCCATTGTGTATGCAGC	ACATGTTCAGCTTTGTGGACC
NRF2	TCTTGGAGTAAGTCGAGAAGTGT	GTTGAAACTGAGCGAAAAAGGC
NQO1	ATGGGAGGTGGTCGAATCTGA	GCCTTCCTTATACGCCAGAGATG
GSTP1	ATGCCACCATACACCATTGTC	GGGAGCTGCCCATACAGAC
GCLC	GGGGTGACGAGGTGGAGT	GTTGGGGTTTGTCCTCTCCC

Table S2□ Information of Patients

	Normal	ALI	Fibrosis	HCC
Number of patients	6	6	6	6
Age	42.67±9.41	43.33±15.69	50.50±12.79	49.00±10.12
Gender (male: female)	2:1	1:2	2:1	1:2
ALT(U/L)	25.21±11.31	556.94±178.59	141.57±56.12	275.27±99.08
AST(U/L)	16.17±4.12	343.54±166.50	101.00±29.08	245.95±107.30
Bilirubin(μmol/L)	13.88±5.70	204.60±45.40	28.63±7.73	288.17±109.99
Treatment	surgery	biopsy	biopsy	biopsy

Data are presented as the mean ± SD

Table S3□ DEGs of TAK1$^{\Delta HEP}$ hepatocyte cluster 7

	p_value	avg_log2FC	pct.1	pct.2	p_value adjust
Prelp	0	0.797101031	0.284	0.006	0
Slpi	0	1.858497355	0.537	0.025	0
S100a11	0	0.958553873	0.456	0.026	0
Osbpl3	0	0.845054691	0.353	0.01	0
Mfge8	0	1.414348694	0.484	0.023	0
Bicc1	0	0.790723677	0.378	0.015	0
Cd63	0	1.53332165	0.625	0.058	0
Ubd	0	1.060237398	0.431	0.011	0
Sox4	1.14E-301	1.035860402	0.303	0.009	2.42E-297
Cd14	4.83E-289	0.680249371	0.266	0.006	1.02E-284
Cybb	3.20E-280	1.214518517	0.484	0.035	6.78E-276
Tagln2	2.45E-274	1.325467013	0.55	0.049	5.20E-270
Anxa2	4.22E-273	1.13882899	0.447	0.03	8.95E-269
Spp1	9.49E-267	4.607928701	0.631	0.074	2.01E-262
Spink1	1.43E-257	1.276282901	0.409	0.026	3.02E-253
Nid1	6.70E-248	0.858957696	0.431	0.031	1.42E-243
Lcn2	4.11E-246	2.797249993	0.794	0.136	8.71E-242
Klf6	1.05E-244	1.019578201	0.481	0.041	2.22E-240
Tes	5.78E-239	0.490005671	0.269	0.01	1.23E-234
Serpina7	1.91E-235	1.800899659	0.469	0.042	4.04E-231
Rad51b	6.50E-222	0.691143361	0.291	0.014	1.38E-217
Ly6d	1.76E-216	2.179541245	0.588	0.075	3.73E-212
Atp6v0c	5.48E-213	1.30405661	0.672	0.099	1.16E-208
Casp12	9.11E-210	0.474411352	0.259	0.011	1.93E-205
Tmsb10	8.99E-209	0.727422063	0.297	0.016	1.91E-204
Serpinb6b	3.60E-204	0.73094084	0.331	0.021	7.64E-200
Cd9	1.48E-203	1.459271378	0.609	0.088	3.13E-199
Rragd	8.96E-202	0.426296742	0.266	0.013	1.90E-197
Serpinb6a	2.91E-195	0.750945891	0.378	0.031	6.16E-191
Slc25a4	4.06E-186	0.491608418	0.281	0.016	8.61E-182
Atp5mpl	5.40E-185	1.229242638	0.744	0.128	1.15E-180
Plscr1	3.27E-183	1.196865761	0.578	0.084	6.93E-179
Tgm2	1.30E-180	1.245674815	0.659	0.111	2.75E-176
Rhoc	2.56E-179	0.630814004	0.381	0.034	5.43E-175
Ifi27l2b	9.70E-178	0.693039057	0.381	0.035	2.06E-173
Gipc2	6.96E-174	0.424083999	0.259	0.015	1.48E-169
Rab5if	1.41E-173	1.044021398	0.637	0.103	2.99E-169
Scd2	1.82E-171	1.139433487	0.472	0.056	3.85E-167
Spon2	1.28E-170	0.56807136	0.35	0.03	2.71E-166
Tnfrsf12a	1.89E-164	0.499537279	0.297	0.022	4.00E-160

Anxa5	1.03E-162	2.087655464	0.784	0.204	2.19E-158
Elf3	1.93E-160	0.471903165	0.259	0.017	4.10E-156
Resf1	6.36E-159	0.544729926	0.319	0.027	1.35E-154
Tut4	2.41E-154	0.488101504	0.306	0.025	5.10E-150
Cystm1	1.60E-153	0.867547233	0.541	0.084	3.40E-149
Tax1bp3	1.61E-150	0.520600174	0.353	0.035	3.42E-146
Tut7	1.05E-148	0.625310571	0.431	0.054	2.23E-144
Stmn1	5.12E-146	0.89976965	0.347	0.036	1.08E-141
Gm30692	8.19E-144	0.501659851	0.259	0.019	1.74E-139
AC102496.1	1.11E-142	0.427597977	0.297	0.026	2.36E-138
Itih5	2.69E-139	0.658668251	0.441	0.059	5.70E-135
Slc39a4	3.35E-139	0.75034716	0.484	0.072	7.09E-135
Cstb	4.65E-137	1.712247762	0.734	0.199	9.86E-133
Lpl	1.20E-133	1.087807865	0.613	0.119	2.55E-129
Saa2	3.35E-132	2.819774034	0.628	0.133	7.11E-128
Sirpa	1.95E-131	0.395801546	0.272	0.023	4.13E-127
Cib3	1.49E-125	0.969489219	0.491	0.083	3.15E-121
Lgals1	2.79E-125	0.780574267	0.409	0.058	5.92E-121
Ciao2a	3.96E-125	0.635795775	0.434	0.064	8.39E-121
Orm2	5.08E-125	2.037785243	0.578	0.125	1.08E-120
Pgm1	1.19E-123	0.592141061	0.475	0.076	2.52E-119
Ifngr1	2.27E-123	0.492167657	0.347	0.041	4.82E-119
Col4a1	7.33E-123	0.370708213	0.25	0.021	1.55E-118
Ly6e	2.71E-121	1.57645702	0.925	0.434	5.74E-117
Tm4sf4	4.24E-121	1.986565198	0.766	0.249	9.00E-117
Tmem176b	1.32E-120	1.916099501	0.841	0.35	2.80E-116
Hpx	1.67E-120	2.020144348	0.994	0.932	3.53E-116
Depp1	1.92E-120	0.581388961	0.347	0.043	4.07E-116
Mvp	7.83E-116	0.477864708	0.328	0.04	1.66E-111
Tubb5	9.22E-116	1.156778764	0.606	0.138	1.95E-111
Ets2	6.15E-115	0.535451574	0.35	0.045	1.30E-110
H2-Q7	1.27E-114	0.835998862	0.606	0.131	2.70E-110
Ndrg1	2.41E-112	0.433813995	0.319	0.038	5.12E-108
B4galt5	2.33E-111	0.5123126	0.344	0.045	4.94E-107
Tmem176a	5.13E-111	1.562149547	0.838	0.361	1.09E-106
Ugt2b37	6.56E-110	0.544975181	0.253	0.025	1.39E-105
Alcam	3.62E-107	1.280587749	0.684	0.197	7.66E-103
Fam124a	7.92E-107	0.390158411	0.253	0.025	1.68E-102
Cxadr	2.57E-106	1.395628059	0.816	0.308	5.46E-102
Sox9	2.77E-106	0.728119153	0.422	0.07	5.86E-102
Rras	8.42E-105	0.631631107	0.444	0.078	1.78E-100
Hp	1.07E-104	1.658749015	0.994	0.93	2.26E-100
Defb1	2.00E-103	0.596038776	0.278	0.032	4.24E-99

Lmna	3.65E-102	0.616115144	0.462	0.084	7.74E-98
Wfdc2	4.26E-101	0.569744215	0.309	0.04	9.02E-97
Slc10a2	1.44E-99	0.756552639	0.55	0.121	3.06E-95
Krt8	1.50E-99	1.890329226	0.812	0.347	3.19E-95
St6gal1	3.79E-99	0.677186994	0.522	0.107	8.03E-95
Clu	2.65E-98	2.570635887	0.963	0.788	5.62E-94
Kifc3	3.48E-98	0.424097044	0.269	0.031	7.37E-94
Kcnq1ot1	1.83E-97	0.954336267	0.559	0.134	3.88E-93
Krt18	5.43E-97	1.609053952	0.812	0.326	1.15E-92
Nfe2l2	2.13E-96	0.734520277	0.537	0.118	4.52E-92
Ppl	2.42E-96	0.403712123	0.294	0.038	5.14E-92
Tpm1	1.20E-95	0.589647954	0.434	0.08	2.54E-91
Myl12a	9.57E-95	1.028615511	0.672	0.194	2.03E-90
Dynll1	1.21E-94	1.092767645	0.744	0.236	2.58E-90
Arpc1b	1.53E-94	0.518602508	0.409	0.072	3.24E-90
Jpt1	9.71E-94	0.563219571	0.366	0.06	2.06E-89
Ramac	3.41E-93	0.378547656	0.275	0.035	7.22E-89
Cp	7.06E-93	1.418220287	0.984	0.784	1.50E-88
Ecpas	2.26E-92	0.310539414	0.25	0.029	4.79E-88
Rbp1	6.23E-92	0.756935991	0.55	0.129	1.32E-87
Isg15	7.15E-92	1.479412355	0.291	0.04	1.52E-87
Mpeg1	1.92E-90	0.495605958	0.338	0.052	4.07E-86
Steap4	2.86E-90	1.211359626	0.65	0.189	6.06E-86
Gstm3	1.39E-88	1.315782535	0.444	0.093	2.95E-84
Pgd	1.92E-88	0.445622954	0.366	0.061	4.08E-84
Birc2	2.03E-88	0.547869425	0.341	0.054	4.30E-84
Ahnak	3.75E-88	0.554935127	0.353	0.058	7.95E-84
Lsr	1.15E-87	0.947246445	0.684	0.208	2.44E-83
Shisa5	8.92E-87	0.425888123	0.35	0.057	1.89E-82
Eif6	2.65E-86	0.726917138	0.619	0.164	5.61E-82
Mmp15	2.85E-86	0.366300683	0.322	0.049	6.04E-82
Fat1	4.45E-86	0.471331228	0.341	0.055	9.44E-82
Map3k1	1.14E-85	0.432660571	0.309	0.046	2.43E-81
Cldn3	3.23E-85	0.900976181	0.603	0.168	6.84E-81
Vnn1	4.94E-85	0.447584143	0.275	0.037	1.05E-80
App	8.91E-85	0.654373729	0.397	0.076	1.89E-80
Dsp	3.78E-84	0.492454451	0.397	0.074	8.01E-80
Saa1	4.32E-84	2.567253311	0.787	0.305	9.17E-80
Ablim1	1.37E-83	0.500402231	0.412	0.08	2.90E-79
Gas6	1.79E-83	0.448273942	0.269	0.037	3.80E-79
Myh9	3.56E-83	0.609146533	0.478	0.105	7.54E-79
Plpp2	6.42E-83	0.439410915	0.341	0.057	1.36E-78
Desi2	2.82E-82	0.56865687	0.566	0.139	5.97E-78

Rhou	4.06E-82	0.72440178	0.603	0.161	8.61E-78
Ahsg	4.13E-82	1.041109697	0.997	0.989	8.76E-78
Tpm4	1.32E-81	0.327956481	0.262	0.035	2.81E-77
Tns3	1.92E-79	0.31157425	0.259	0.035	4.06E-75
Nav2	3.00E-79	0.465671421	0.375	0.07	6.37E-75
Cd2ap	5.30E-79	0.760419264	0.569	0.153	1.12E-74
Samd9l	6.64E-79	0.337908707	0.275	0.04	1.41E-74
Ywhah	1.48E-78	0.781055882	0.603	0.17	3.13E-74
Pdlim1	1.68E-77	0.45404857	0.428	0.089	3.56E-73
Igtp	2.47E-77	0.561718971	0.25	0.034	5.25E-73
Mapk3	1.05E-76	0.375048456	0.3	0.048	2.23E-72
Gc	1.73E-76	0.783505512	1	0.98	3.66E-72
Colgalt1	1.25E-74	0.568586189	0.503	0.122	2.66E-70
9-Sep	2.48E-74	0.517286001	0.472	0.109	5.25E-70
Slc4a4	7.74E-74	0.813720093	0.7	0.228	1.64E-69
Itm2c	6.55E-73	0.365760372	0.297	0.049	1.39E-68
Ntrk2	2.22E-72	0.364896799	0.25	0.036	4.71E-68
Ppp4c	5.99E-72	0.414538832	0.403	0.085	1.27E-67
Atpif1	7.75E-72	0.670108478	0.556	0.153	1.64E-67
Dag1	9.63E-72	0.6661454	0.494	0.126	2.04E-67
Mgst3	5.53E-71	0.427659318	0.344	0.066	1.17E-66
Serpina10	1.02E-69	0.88672363	0.772	0.306	2.17E-65
Chmp2b	1.19E-69	0.440147156	0.444	0.102	2.52E-65
Irgm2	1.46E-68	0.458849816	0.281	0.047	3.11E-64
Tceal9	2.81E-68	0.521660635	0.403	0.091	5.96E-64
Eppk1	4.29E-68	0.37993259	0.369	0.075	9.10E-64
Hsd17b13	6.48E-68	1.440167112	0.831	0.453	1.37E-63
Rtn4	8.23E-68	1.136424149	0.694	0.268	1.74E-63
Serinc5	9.69E-68	0.367429582	0.344	0.067	2.05E-63
Rnf213	1.37E-67	0.524422182	0.359	0.075	2.90E-63
Otud7b	7.92E-67	0.273854236	0.284	0.048	1.68E-62
Nostrin	8.88E-67	0.349410233	0.319	0.06	1.88E-62
Slc6a6	1.24E-66	0.711443285	0.672	0.211	2.63E-62
Gars	1.71E-66	0.347936407	0.341	0.067	3.62E-62
C3	8.27E-66	1.20701631	0.981	0.924	1.75E-61
Myl12b	2.90E-65	0.585047272	0.562	0.162	6.14E-61
Cd47	3.17E-65	0.820428032	0.753	0.283	6.73E-61
Baiap2	3.53E-65	0.346580517	0.359	0.074	7.49E-61
Nedd4l	8.20E-65	0.529507231	0.484	0.127	1.74E-60
Mt2	1.00E-64	0.833162122	0.497	0.139	2.12E-60
Serping1	1.06E-64	0.935923034	0.931	0.591	2.25E-60
Ambp	2.51E-64	0.865833236	0.981	0.846	5.33E-60
Cyr61	1.23E-63	0.500966558	0.266	0.046	2.61E-59

Ifi47	4.20E-63	0.719673648	0.334	0.07	8.90E-59
Cadm1	6.43E-63	0.433709996	0.378	0.084	1.36E-58
Nectin2	7.12E-63	0.463743621	0.416	0.099	1.51E-58
Med21	1.27E-62	0.515657649	0.525	0.147	2.68E-58
Sqstm1	3.17E-62	0.721178955	0.647	0.218	6.73E-58
Asah1	5.31E-62	0.377648762	0.366	0.08	1.13E-57
Arhgdia	4.60E-61	0.395128969	0.409	0.097	9.76E-57
Reep5	5.90E-61	0.353824831	0.391	0.09	1.25E-56
Trf	2.80E-60	0.784457428	1	0.998	5.94E-56
Srxn1	5.07E-60	0.37435423	0.278	0.051	1.08E-55
Hacd2	5.89E-60	0.477704433	0.494	0.135	1.25E-55
Ddx39b	2.86E-59	0.367329582	0.362	0.081	6.07E-55
Anxa7	4.91E-59	0.447659838	0.531	0.151	1.04E-54
Tpr	5.36E-59	0.555177479	0.547	0.166	1.14E-54
Spint2	7.22E-59	0.636949446	0.591	0.194	1.53E-54
Tspo	1.24E-58	0.746264713	0.716	0.284	2.63E-54
Gss	1.58E-58	0.429621009	0.428	0.109	3.34E-54
Psme1	3.03E-58	0.559149166	0.622	0.204	6.42E-54
Uhrf2	3.63E-58	0.366582566	0.378	0.088	7.69E-54
Ppia	7.43E-58	0.821411847	0.978	0.845	1.58E-53
Gstm5	7.50E-58	0.369649987	0.303	0.062	1.59E-53
Frrs1	7.63E-58	0.420329855	0.419	0.106	1.62E-53
Npc2	1.07E-57	0.587791589	0.606	0.199	2.28E-53
Crip2	1.45E-57	0.569514393	0.559	0.174	3.07E-53
Ifitm3	2.01E-57	0.730474864	0.991	0.886	4.27E-53
Cd151	2.89E-57	0.305846257	0.272	0.051	6.14E-53
Sorbs2	5.33E-57	0.966195857	0.691	0.284	1.13E-52
Sqle	7.20E-57	0.475676792	0.406	0.103	1.53E-52
Idh2	9.82E-57	0.493410901	0.575	0.179	2.08E-52
Ube2v2	1.24E-56	0.606256898	0.459	0.13	2.64E-52
Tbrg1	2.15E-56	0.406972846	0.406	0.102	4.57E-52
Hspa4l	3.03E-56	0.409146065	0.362	0.085	6.43E-52
Acsl4	3.48E-56	0.592243758	0.6	0.198	7.37E-52
H2-D1	4.18E-56	0.925614942	0.875	0.486	8.85E-52
Apcs	5.06E-56	0.868227104	0.681	0.257	1.07E-51
Atp6v0e	7.34E-56	0.717217701	0.697	0.269	1.56E-51
Grn	3.19E-55	0.680386245	0.625	0.22	6.77E-51
Trp53	9.14E-55	0.25523345	0.269	0.051	1.94E-50
Fkbp1a	1.21E-54	0.605013049	0.606	0.206	2.56E-50
Cobl	1.51E-54	0.286555639	0.275	0.053	3.19E-50
Sat1	1.55E-54	0.639384738	0.641	0.229	3.28E-50
Lgmn	2.42E-54	0.380826038	0.306	0.065	5.12E-50
Rock2	6.72E-54	0.353471533	0.381	0.094	1.43E-49

Pbx1	6.89E-54	0.341015491	0.278	0.056	1.46E-49
Hspb1	1.02E-53	0.498982768	0.291	0.061	2.17E-49
Dnajc10	1.27E-53	0.270767035	0.259	0.049	2.70E-49
Atp9a	4.01E-53	0.300739391	0.291	0.06	8.49E-49
Mrps6	4.55E-53	0.255895734	0.306	0.065	9.64E-49
Ephx1	6.46E-53	0.496588389	0.528	0.162	1.37E-48
Gnb1	6.68E-53	0.485304334	0.559	0.178	1.42E-48
AW112010	1.14E-52	1.06224174	0.884	0.477	2.42E-48
Myo10	1.24E-52	0.284506801	0.309	0.067	2.63E-48
Ccl9	1.31E-52	0.770785719	0.631	0.232	2.79E-48
Akap13	1.66E-52	0.508951286	0.466	0.136	3.51E-48
Lima1	1.97E-52	0.373010718	0.359	0.087	4.18E-48
Tnfaip1	2.47E-52	0.272796761	0.3	0.064	5.25E-48
Hdac5	2.80E-52	0.274259672	0.253	0.048	5.94E-48
Fbxo6	3.05E-52	0.359202409	0.353	0.085	6.47E-48
Fkbp11	4.71E-52	0.360192541	0.372	0.093	9.98E-48
Sri	4.98E-52	0.287424751	0.419	0.109	1.06E-47
Plekha5	5.65E-52	0.282933836	0.297	0.063	1.20E-47
Acin1	6.06E-52	0.289519902	0.331	0.076	1.28E-47
Palmd	6.70E-52	0.353509302	0.353	0.085	1.42E-47
Sptan1	6.72E-52	0.330233494	0.278	0.057	1.42E-47
Adgrl2	6.81E-52	0.40287801	0.378	0.096	1.44E-47
Mup20	9.58E-52	1.346015486	1	0.987	2.03E-47
Anxa4	1.74E-51	0.372170244	0.391	0.101	3.69E-47
Adh1	2.96E-51	0.892721438	0.944	0.689	6.27E-47
Ppp1r14b	3.96E-51	0.385057816	0.409	0.11	8.40E-47
Tuba1b	4.02E-51	0.443688782	0.297	0.066	8.52E-47
Trim25	4.34E-51	0.382257342	0.403	0.106	9.19E-47
Dsc2	4.44E-51	0.355552818	0.362	0.089	9.42E-47
Snx10	4.83E-51	0.489951638	0.469	0.139	1.02E-46
Psmb10	7.28E-51	0.286677196	0.347	0.083	1.54E-46
Bax	1.23E-50	0.405303387	0.409	0.111	2.60E-46
St3gal4	1.38E-50	0.431336556	0.419	0.115	2.93E-46
Itgb5	1.85E-50	0.348369835	0.328	0.077	3.93E-46
Glmp	2.12E-50	0.262971814	0.359	0.088	4.49E-46
Pla1a	2.24E-50	0.361952145	0.378	0.097	4.74E-46
Ccnd1	2.29E-50	0.476122303	0.303	0.07	4.85E-46
Sugt1	2.36E-50	0.290821384	0.372	0.093	5.00E-46
Micu2	2.42E-50	0.262777924	0.291	0.062	5.13E-46
Rnpep	2.94E-50	0.292242475	0.284	0.06	6.24E-46
Gng12	3.44E-50	0.417327994	0.55	0.173	7.29E-46
Cxcl14	4.22E-50	0.459596263	0.294	0.065	8.95E-46
Slc35f5	4.71E-50	0.334427182	0.369	0.093	9.99E-46

Arl6ip5	5.39E-50	0.284533785	0.278	0.058	1.14E-45
Litaf	5.60E-50	0.569131384	0.616	0.222	1.19E-45
Gnai2	5.95E-50	0.386101809	0.45	0.129	1.26E-45
Creb3l2	1.42E-49	0.349270619	0.312	0.072	3.02E-45
Mpp1	1.49E-49	0.269361772	0.319	0.074	3.15E-45
Rhod	1.53E-49	0.267167436	0.306	0.069	3.24E-45
Mbd2	2.19E-49	0.328209585	0.45	0.127	4.64E-45
Ctnna1	2.80E-49	0.417559306	0.522	0.162	5.93E-45
Gstm1	3.21E-49	1.264601432	0.938	0.793	6.81E-45
Gpx4	3.25E-49	0.833008521	0.925	0.677	6.89E-45
Maged1	3.81E-49	0.475403022	0.491	0.151	8.08E-45
Fndc3b	5.03E-49	0.441453475	0.456	0.135	1.07E-44
Ago2	6.25E-49	0.264304619	0.272	0.057	1.32E-44
Phip	6.73E-49	0.303409841	0.334	0.08	1.43E-44
Cnih4	1.53E-48	0.380065748	0.384	0.102	3.23E-44
Mob1a	1.56E-48	0.302499995	0.378	0.097	3.31E-44
Acsl3	1.92E-48	0.263280818	0.3	0.068	4.08E-44
Calu	2.12E-48	0.464453555	0.5	0.155	4.50E-44
Tmpo	2.91E-48	0.387247242	0.375	0.099	6.17E-44
Selenoh	3.03E-48	0.370326825	0.266	0.056	6.42E-44
Ttc3	4.85E-48	0.319370297	0.275	0.06	1.03E-43
Hspa8	5.73E-48	0.829868153	0.95	0.749	1.22E-43
Lgals3bp	6.06E-48	0.364036312	0.331	0.082	1.29E-43
Pcsk9	9.88E-48	0.309783321	0.256	0.053	2.10E-43
Tubb2a	1.48E-47	0.541130765	0.644	0.243	3.14E-43
Serinc3	1.68E-47	0.690643586	0.766	0.345	3.55E-43
Gcnt2	2.03E-47	0.34596213	0.253	0.052	4.31E-43
Snrpc	2.55E-47	0.275101002	0.416	0.114	5.41E-43
Gm10073	3.72E-47	0.28731513	0.281	0.063	7.88E-43
Fgl1	4.76E-47	0.912889594	0.809	0.398	1.01E-42
Tra2a	6.21E-47	0.299892488	0.334	0.083	1.32E-42
Cdh1	1.04E-46	0.482169825	0.553	0.186	2.21E-42
Diaph1	1.31E-46	0.4153069	0.431	0.127	2.78E-42
Cdk6	1.37E-46	0.343463664	0.322	0.079	2.90E-42
Hnrnpa1	1.38E-46	0.402963349	0.425	0.123	2.92E-42
Tapbp	1.61E-46	0.452196185	0.491	0.155	3.40E-42
Map3k13	1.73E-46	0.251690152	0.256	0.054	3.67E-42
Serpinc1	1.78E-46	0.751856529	0.972	0.799	3.77E-42
P2rx4	3.13E-46	0.33818116	0.309	0.074	6.64E-42
Cr1l	3.96E-46	0.318473548	0.331	0.083	8.39E-42
Med28	4.41E-46	0.350049082	0.359	0.095	9.36E-42
Raph1	5.24E-46	0.661983825	0.666	0.269	1.11E-41
Ctsl	6.36E-46	0.779948416	0.919	0.618	1.35E-41

Nabp1	6.43E-46	0.286558499	0.256	0.054	1.36E-41
Commd2	6.53E-46	0.277427572	0.309	0.074	1.38E-41
C2	7.19E-46	0.370045975	0.478	0.146	1.52E-41
Wnk1	1.19E-45	0.483124671	0.588	0.209	2.52E-41
Mt1	1.45E-45	1.058006368	0.8	0.413	3.07E-41
Pmvk	2.59E-45	0.465221007	0.519	0.174	5.50E-41
Cct4	2.87E-45	0.447117735	0.603	0.215	6.08E-41
Ptprj	3.27E-45	0.287681329	0.316	0.077	6.94E-41
Tnfrsf1a	4.16E-45	0.285787092	0.375	0.102	8.81E-41
Tspan4	5.34E-45	0.346082833	0.388	0.109	1.13E-40
Cd36	6.33E-45	0.345601603	0.278	0.064	1.34E-40
Atp1b1	6.99E-45	0.455271002	0.453	0.141	1.48E-40
Actg1	7.90E-45	0.881000979	0.734	0.352	1.67E-40
Tstd1	9.09E-45	0.483399593	0.372	0.104	1.93E-40
Fn1	9.67E-45	0.723246662	0.966	0.766	2.05E-40
Lims1	1.06E-44	0.279108227	0.278	0.063	2.24E-40
Fdft1	1.25E-44	0.43082784	0.45	0.139	2.64E-40
Spcs1	1.30E-44	0.675626426	0.787	0.381	2.76E-40
Nfkb1	1.43E-44	0.32634042	0.253	0.055	3.02E-40
Tcim	2.38E-44	0.383301072	0.438	0.133	5.05E-40
Bag3	2.50E-44	0.334629013	0.312	0.078	5.31E-40
Cfdp1	2.51E-44	0.340248115	0.45	0.137	5.32E-40
Rpl27	3.47E-44	0.705457086	0.838	0.456	7.37E-40
Mbnl2	4.79E-44	0.397008161	0.409	0.121	1.02E-39
B2m	4.88E-44	0.566642071	1	0.949	1.04E-39
Maea	5.22E-44	0.287756964	0.275	0.063	1.11E-39
Pdcl3	7.18E-44	0.264722505	0.319	0.08	1.52E-39
Cnn3	1.77E-43	0.531220635	0.637	0.247	3.75E-39
Lrif1	2.04E-43	0.26959849	0.253	0.055	4.31E-39
Stbd1	2.38E-43	0.299927049	0.356	0.096	5.04E-39
Mdfic	2.38E-43	0.287407469	0.3	0.073	5.06E-39
Dsg2	2.49E-43	0.456190627	0.55	0.19	5.28E-39
Tmem97	2.58E-43	0.401417816	0.438	0.134	5.47E-39
Twsg1	3.00E-43	0.326278911	0.362	0.099	6.37E-39
Mat2a	3.85E-43	0.403548323	0.503	0.165	8.16E-39
Aqp8	5.21E-43	0.641740166	0.588	0.227	1.10E-38
Gm26917	5.22E-43	0.253015944	0.344	0.091	1.11E-38
Hexa	5.27E-43	0.260013746	0.284	0.068	1.12E-38
Rrp1	6.43E-43	0.282253654	0.403	0.116	1.36E-38
Bub3	6.44E-43	0.273884192	0.306	0.076	1.36E-38
Itih2	6.82E-43	0.790508707	0.853	0.525	1.45E-38
Nck1	7.32E-43	0.325135854	0.316	0.081	1.55E-38
Lrg1	7.46E-43	0.978058401	0.897	0.621	1.58E-38

Zfp950	1.10E-42	0.259178355	0.284	0.068	2.33E-38
Arf3	1.40E-42	0.315656282	0.431	0.129	2.97E-38
Mcl1	1.41E-42	0.414603649	0.534	0.184	3.00E-38
Cebpg	1.71E-42	0.365236416	0.403	0.12	3.62E-38
Vps29	2.24E-42	0.358647241	0.503	0.167	4.74E-38
Vtn	2.45E-42	0.715304958	0.972	0.833	5.20E-38
Cdc42	2.59E-42	0.610692277	0.741	0.34	5.50E-38
Vnn3	2.94E-42	0.26997184	0.281	0.067	6.24E-38
AC149090.1	3.60E-42	0.272383635	0.288	0.069	7.62E-38
Ifitm2	3.70E-42	0.686302061	0.872	0.493	7.84E-38
Nisch	3.97E-42	0.369047061	0.459	0.145	8.42E-38
Prdx4	5.61E-42	0.604173223	0.694	0.299	1.19E-37
Gnb2	5.95E-42	0.476910986	0.594	0.224	1.26E-37
Ctnnd1	8.55E-42	0.420982298	0.481	0.159	1.81E-37
Hnrnpm	9.36E-42	0.293982777	0.444	0.136	1.98E-37
Slc17a4	1.14E-41	0.299756324	0.356	0.098	2.43E-37
Psme2	1.74E-41	0.352067362	0.55	0.191	3.69E-37
Adam10	1.75E-41	0.256670817	0.3	0.075	3.71E-37
Dusp16	2.11E-41	0.329196272	0.303	0.078	4.48E-37
Tkt	2.32E-41	0.367728185	0.503	0.168	4.93E-37
G3bp2	3.13E-41	0.494932513	0.634	0.242	6.63E-37
Rnh1	4.51E-41	0.36840027	0.478	0.159	9.55E-37
Afdn	9.25E-41	0.277588759	0.35	0.097	1.96E-36
Alyref	1.02E-40	0.294897791	0.322	0.086	2.17E-36
Gsta4	1.11E-40	0.353349406	0.459	0.149	2.35E-36
Nrip1	1.24E-40	0.30779936	0.328	0.088	2.62E-36
Ube2z	1.26E-40	0.253908314	0.331	0.089	2.67E-36
Ptma	1.32E-40	0.774196475	0.938	0.708	2.79E-36
Itgb1	1.52E-40	0.428579791	0.559	0.201	3.23E-36
Csad	1.70E-40	0.787936082	0.597	0.251	3.61E-36
Myl6	2.35E-40	0.695948751	0.859	0.545	4.99E-36
Rdh11	3.53E-40	0.279702523	0.291	0.073	7.48E-36
Itgav	3.54E-40	0.364612268	0.306	0.081	7.50E-36
Cst3	4.03E-40	0.560171624	0.781	0.364	8.54E-36
H2-K1	4.04E-40	0.607820952	0.988	0.849	8.57E-36
Sptbn1	4.13E-40	0.347019098	0.391	0.118	8.76E-36
Vps28	4.39E-40	0.340804844	0.462	0.151	9.31E-36
Abhd2	4.68E-40	0.299707134	0.378	0.11	9.92E-36
Gusb	5.18E-40	0.272311977	0.269	0.065	1.10E-35
Calm2	5.38E-40	0.649522971	0.759	0.381	1.14E-35
Zbtb20	5.91E-40	0.801341601	0.922	0.654	1.25E-35
Mug2	7.31E-40	0.728763597	0.806	0.403	1.55E-35
Eef1a1	7.70E-40	0.519356787	1	0.988	1.63E-35

Chka	8.95E-40	0.605644083	0.662	0.279	1.90E-35
Cpq	9.52E-40	0.381073802	0.462	0.153	2.02E-35
Cox19	1.16E-39	0.356934531	0.45	0.147	2.45E-35
Abcb4	1.79E-39	0.517688371	0.597	0.235	3.80E-35
Hax1	1.81E-39	0.250298482	0.372	0.107	3.83E-35
Lasp1	2.31E-39	0.364157763	0.591	0.215	4.89E-35
Plin3	2.62E-39	0.250123659	0.303	0.079	5.55E-35
4930402H24Rik	3.17E-39	0.253620284	0.3	0.078	6.71E-35
Psmd8	3.20E-39	0.542534885	0.697	0.304	6.78E-35
Ermp1	3.47E-39	0.252104535	0.25	0.058	7.35E-35
Banf1	4.51E-39	0.297203786	0.391	0.118	9.57E-35
Bcap31	5.88E-39	0.466308313	0.681	0.276	1.25E-34
Nop58	8.07E-39	0.254457673	0.272	0.067	1.71E-34
H13	8.39E-39	0.447670899	0.566	0.213	1.78E-34
Nap1l1	9.17E-39	0.52610077	0.588	0.229	1.94E-34
Ik	1.00E-38	0.270249378	0.406	0.125	2.12E-34
Hsp90aa1	1.15E-38	0.812931538	0.803	0.471	2.44E-34
Slc16a1	1.34E-38	0.340788651	0.375	0.113	2.84E-34
Hnrnph1	1.36E-38	0.305316047	0.459	0.15	2.87E-34
Ifrd1	1.55E-38	0.286125249	0.269	0.066	3.29E-34
Dnajc1	1.65E-38	0.260309388	0.35	0.1	3.50E-34
Acp5	2.52E-38	0.402357653	0.5	0.177	5.34E-34
Fasn	2.84E-38	0.448090466	0.566	0.209	6.03E-34
Tuba1c	4.25E-38	0.330053745	0.362	0.109	9.01E-34
Bmpr1a	4.30E-38	0.263295559	0.291	0.075	9.12E-34
Nectin1	4.64E-38	0.312977595	0.369	0.11	9.85E-34
Chdh	4.87E-38	0.301497913	0.4	0.124	1.03E-33
Agl	5.28E-38	0.258227779	0.253	0.061	1.12E-33
Vwa5a	1.29E-37	0.304070204	0.278	0.071	2.74E-33
Hmgn1	1.52E-37	0.577941832	0.694	0.316	3.22E-33
Kdm2a	2.48E-37	0.266423008	0.369	0.11	5.25E-33
Capns1	2.82E-37	0.411284048	0.544	0.202	5.98E-33
Trip11	2.84E-37	0.262622372	0.356	0.104	6.01E-33
Krit1	3.03E-37	0.279033652	0.312	0.086	6.42E-33
Pkp2	3.12E-37	0.259109367	0.294	0.078	6.60E-33
St5	3.26E-37	0.261079052	0.328	0.093	6.90E-33
Clptm1	3.37E-37	0.308911377	0.359	0.108	7.15E-33
Hsp90ab1	3.61E-37	0.692097365	0.953	0.778	7.65E-33
Srsf7	3.81E-37	0.26847996	0.338	0.098	8.08E-33
Dmd	4.98E-37	0.251048194	0.284	0.074	1.05E-32
Cct7	6.03E-37	0.304713531	0.469	0.16	1.28E-32
Pon2	7.24E-37	0.274479061	0.456	0.151	1.54E-32
Eif3l	7.80E-37	0.33978541	0.447	0.151	1.65E-32

Tsen34	1.03E-36	0.268505939	0.344	0.101	2.19E-32
Hikeshi	1.29E-36	0.254007199	0.359	0.107	2.73E-32
Sec11a	1.36E-36	0.432646522	0.562	0.218	2.89E-32
Ddost	2.04E-36	0.348899515	0.45	0.154	4.32E-32
Jak1	3.13E-36	0.341329016	0.537	0.197	6.64E-32
Stt3b	3.20E-36	0.362756756	0.512	0.187	6.79E-32
Nsdhl	3.28E-36	0.334915417	0.369	0.114	6.96E-32
Irf6	6.40E-36	0.286363329	0.372	0.114	1.36E-31
Thoc7	6.61E-36	0.384417412	0.569	0.215	1.40E-31
Ssrp1	7.31E-36	0.273098057	0.344	0.102	1.55E-31
Socs2	7.41E-36	0.301373244	0.269	0.071	1.57E-31
Ptprf	8.60E-36	0.452414133	0.603	0.242	1.82E-31
Tm2d3	1.15E-35	0.2734998	0.338	0.1	2.44E-31
Abracl	1.50E-35	0.259351924	0.344	0.102	3.19E-31
Sh3d19	1.54E-35	0.270017689	0.394	0.125	3.26E-31
Jkamp	1.97E-35	0.252719496	0.309	0.087	4.17E-31
Cpn1	2.00E-35	0.440802177	0.725	0.315	4.24E-31
Prg4	2.00E-35	0.300039723	0.256	0.065	4.25E-31
Psma2	2.66E-35	0.285037445	0.659	0.26	5.64E-31
C4bp	2.80E-35	0.635954782	0.956	0.713	5.94E-31
Cfl1	3.88E-35	0.417951232	0.669	0.284	8.22E-31
Eif3m	4.43E-35	0.359569545	0.578	0.223	9.39E-31
Plec	4.84E-35	0.261040885	0.284	0.077	1.03E-30
Tubb4b	8.65E-35	0.758803033	0.506	0.203	1.83E-30
C6	9.42E-35	0.463545511	0.534	0.21	2.00E-30
Drg1	1.32E-34	0.281500683	0.362	0.112	2.80E-30
Polr2k	1.41E-34	0.363465709	0.559	0.214	2.99E-30
Fubp1	1.70E-34	0.325090936	0.344	0.106	3.59E-30
Rbms1	1.79E-34	0.260907514	0.366	0.113	3.79E-30
Clint1	3.07E-34	0.30749265	0.475	0.168	6.50E-30
Psmd7	3.61E-34	0.3384749	0.519	0.193	7.66E-30
Sh3glb1	3.77E-34	0.316744758	0.566	0.215	7.98E-30
Ostf1	3.79E-34	0.281088788	0.394	0.13	8.03E-30
Zc3hav1	4.09E-34	0.281706328	0.359	0.112	8.66E-30
B4galnt1	4.37E-34	0.281948496	0.388	0.125	9.27E-30
Nedd4	4.57E-34	0.49389531	0.672	0.299	9.69E-30
Sfpq	5.45E-34	0.338977934	0.481	0.174	1.16E-29
M6pr	5.68E-34	0.28765868	0.422	0.142	1.20E-29
Itih3	5.71E-34	0.652167752	0.872	0.545	1.21E-29
Rbm5	6.37E-34	0.258056381	0.309	0.09	1.35E-29
Cct5	6.59E-34	0.339026673	0.544	0.209	1.40E-29
Tmbim4	7.25E-34	0.396160519	0.675	0.287	1.54E-29
Slc22a18	1.03E-33	0.344702838	0.406	0.138	2.18E-29

Mgam	1.05E-33	0.252289372	0.35	0.108	2.22E-29
Rnf139	1.05E-33	0.255095568	0.3	0.086	2.23E-29
Ces2e	1.13E-33	0.541615406	0.559	0.234	2.40E-29
Nipbl	1.15E-33	0.271581131	0.378	0.121	2.44E-29
Zfand3	1.33E-33	0.254936374	0.403	0.133	2.81E-29
Cct8	1.61E-33	0.27550315	0.584	0.226	3.42E-29
Htatip2	1.80E-33	0.250790712	0.344	0.106	3.82E-29
Snrpb	1.84E-33	0.338611401	0.466	0.17	3.90E-29
Ddb1	2.08E-33	0.346066682	0.519	0.197	4.41E-29
Eno1	2.08E-33	0.351145215	0.534	0.205	4.41E-29
Jun	2.53E-33	0.462263556	0.522	0.207	5.36E-29
Ubb	2.80E-33	0.457044516	0.863	0.53	5.93E-29
G3bp1	3.34E-33	0.385822281	0.441	0.158	7.09E-29
Stat1	3.94E-33	0.546735504	0.281	0.081	8.36E-29
Psap	5.13E-33	0.623494905	0.731	0.372	1.09E-28
Pglyrp2	5.44E-33	0.356611921	0.441	0.158	1.15E-28
Tsn	6.84E-33	0.330298515	0.522	0.198	1.45E-28
Jmjd1c	7.34E-33	0.27909483	0.394	0.13	1.56E-28
Ssu72	9.92E-33	0.2719336	0.528	0.198	2.10E-28
Nbeal1	1.14E-32	0.299538766	0.512	0.191	2.41E-28
Scarb1	1.25E-32	0.313427375	0.428	0.149	2.65E-28
Prdx1	1.92E-32	0.451719074	0.994	0.935	4.08E-28
Arpc3	2.16E-32	0.251829815	0.522	0.197	4.59E-28
Acaca	2.39E-32	0.284277788	0.338	0.106	5.07E-28
Itih4	2.48E-32	0.641429044	0.944	0.694	5.26E-28
Kmt2e	4.11E-32	0.274671969	0.428	0.149	8.71E-28
Hmgcs1	5.15E-32	0.832564635	0.728	0.394	1.09E-27
H2-T22	7.03E-32	0.256353531	0.431	0.151	1.49E-27
Btg2	7.19E-32	0.522430927	0.531	0.222	1.52E-27
Hnrnpc	7.64E-32	0.308759829	0.575	0.228	1.62E-27
Tmem208	7.97E-32	0.274005569	0.506	0.19	1.69E-27
Tmed9	1.29E-31	0.321727326	0.497	0.188	2.73E-27
Atxn10	1.35E-31	0.281474641	0.456	0.165	2.86E-27
Txnrd1	1.41E-31	0.44878113	0.541	0.221	3.00E-27
Rbbp7	1.58E-31	0.266147346	0.419	0.146	3.36E-27
Ptpn11	1.66E-31	0.268272501	0.341	0.108	3.52E-27
Rab11a	1.94E-31	0.397764491	0.581	0.239	4.12E-27
Mdh2	2.04E-31	0.388348299	0.747	0.346	4.33E-27
Kpnb1	2.06E-31	0.270085264	0.419	0.145	4.36E-27
Laptm4a	2.06E-31	0.513060963	0.778	0.395	4.37E-27
Hjurp	2.20E-31	0.270559777	0.306	0.093	4.66E-27
Nono	2.29E-31	0.352967741	0.509	0.198	4.85E-27
Zmpste24	2.53E-31	0.28370233	0.406	0.141	5.37E-27

Jund	2.55E-31	0.290379318	0.537	0.209	5.41E-27
Dst	3.49E-31	0.341340596	0.4	0.141	7.39E-27
Pcbp1	6.60E-31	0.521298177	0.772	0.406	1.40E-26
Fgb	6.71E-31	0.579305953	1	0.972	1.42E-26
Cfi	7.11E-31	0.55084552	0.916	0.61	1.51E-26
Tpm3	8.45E-31	0.250085793	0.378	0.128	1.79E-26
H2afz	1.00E-30	0.815709761	0.769	0.419	2.13E-26
Abca3	1.13E-30	0.262501227	0.294	0.088	2.40E-26
Dynlt3	1.23E-30	0.364230805	0.537	0.214	2.61E-26
Cct2	1.29E-30	0.306155051	0.544	0.214	2.73E-26
Rtn3	1.32E-30	0.30860054	0.522	0.203	2.79E-26
Tpp1	1.44E-30	0.349549942	0.562	0.226	3.05E-26
Gstm6	1.45E-30	0.306771881	0.506	0.194	3.07E-26
Ywhaz	1.92E-30	0.4565247	0.641	0.286	4.07E-26
Eif4ebp1	2.00E-30	0.305730502	0.497	0.191	4.24E-26
Morf4l2	2.43E-30	0.311361909	0.584	0.236	5.16E-26
Nudt4	2.48E-30	0.541539321	0.734	0.376	5.26E-26
Commd3	2.59E-30	0.324986244	0.541	0.217	5.49E-26
Capzb	3.24E-30	0.311142306	0.5	0.194	6.86E-26
Arid1a	3.44E-30	0.250196389	0.338	0.109	7.30E-26
Pla2g12b	4.12E-30	0.253577098	0.381	0.131	8.74E-26
Ctsa	4.74E-30	0.329910071	0.338	0.112	1.01E-25
Pkp4	5.65E-30	0.266928741	0.397	0.139	1.20E-25
Pabpc1	6.33E-30	0.595882585	0.803	0.461	1.34E-25
Gtf2i	7.74E-30	0.263169164	0.362	0.122	1.64E-25
Fdps	8.11E-30	0.393590096	0.572	0.241	1.72E-25
Csrp2	8.47E-30	0.270971092	0.375	0.129	1.80E-25
Larp4b	8.62E-30	0.47313324	0.706	0.339	1.83E-25
Phf3	1.02E-29	0.263839288	0.359	0.121	2.15E-25
Pros1	1.05E-29	0.266838839	0.362	0.123	2.22E-25
Snrpe	1.09E-29	0.348885346	0.644	0.276	2.31E-25
Cdkn1a	1.14E-29	0.331008912	0.475	0.181	2.41E-25
Sdc1	1.98E-29	0.392225601	0.634	0.28	4.20E-25
Cope	2.11E-29	0.250436975	0.537	0.213	4.47E-25
Rbpms	3.21E-29	0.381208529	0.572	0.242	6.81E-25
Gsta2	3.67E-29	0.267150458	0.291	0.09	7.77E-25
Csnk2b	3.99E-29	0.253780383	0.491	0.19	8.45E-25
Kng2	4.09E-29	0.464973745	0.641	0.295	8.66E-25
Dhcr24	5.19E-29	0.59171938	0.834	0.49	1.10E-24
Atp6v1e1	5.50E-29	0.306931403	0.588	0.244	1.17E-24
Hsp90b1	5.55E-29	0.580755735	0.969	0.78	1.18E-24
Cyp51	5.71E-29	0.450826547	0.525	0.221	1.21E-24
Habp2	5.91E-29	0.289508329	0.428	0.158	1.25E-24

Pzp	7.07E-29	0.574893315	0.919	0.664	1.50E-24
F12	8.70E-29	0.552487242	0.694	0.36	1.84E-24
Net1	9.31E-29	0.25142758	0.306	0.097	1.97E-24
Cast	1.09E-28	0.258893164	0.384	0.134	2.31E-24
Abcc3	1.22E-28	0.27771272	0.431	0.16	2.59E-24
Ssb	1.35E-28	0.252809021	0.478	0.182	2.87E-24
Eif3f	1.65E-28	0.366971952	0.591	0.259	3.50E-24
Manf	2.08E-28	0.594398609	0.787	0.441	4.42E-24
Emc7	2.22E-28	0.280576703	0.528	0.211	4.70E-24
Qk	2.30E-28	0.323252004	0.525	0.212	4.87E-24
Ifih1	2.36E-28	0.259442961	0.325	0.107	5.00E-24
Pdia6	2.89E-28	0.545583959	0.822	0.477	6.14E-24
Slc39a14	3.28E-28	0.325162076	0.553	0.229	6.94E-24
Echdc2	3.55E-28	0.281291009	0.494	0.194	7.52E-24
Tmem50a	3.58E-28	0.268153252	0.475	0.184	7.59E-24
Pbrm1	3.64E-28	0.302763373	0.531	0.213	7.72E-24
Gsk3b	4.05E-28	0.265247303	0.431	0.161	8.59E-24
Qprt	4.29E-28	0.335757118	0.603	0.261	9.09E-24
Pcyox1	5.27E-28	0.294371844	0.475	0.185	1.12E-23
Tecr	5.53E-28	0.408206485	0.681	0.32	1.17E-23
Aplp2	5.78E-28	0.512807302	0.791	0.445	1.22E-23
Ncl	6.29E-28	0.269276225	0.559	0.231	1.33E-23
Ldlr	6.37E-28	0.290312151	0.431	0.162	1.35E-23
Xbp1	6.47E-28	0.475442195	0.759	0.391	1.37E-23
Sdf2l1	1.36E-27	0.293754448	0.444	0.171	2.89E-23
Arpp19	1.53E-27	0.357064504	0.625	0.283	3.24E-23
Clptm1l	1.91E-27	0.259583853	0.431	0.162	4.05E-23
Znrf2	3.13E-27	0.268887185	0.519	0.209	6.64E-23
Srsf3	3.70E-27	0.264513913	0.494	0.196	7.84E-23
Calr	3.73E-27	0.549562635	0.966	0.778	7.90E-23
Ssbp3	3.86E-27	0.292252491	0.409	0.153	8.19E-23
Rps4x	4.54E-27	0.506948936	0.972	0.799	9.63E-23
Nampt	6.20E-27	0.269757688	0.45	0.174	1.32E-22
Pnp	6.92E-27	0.390243671	0.656	0.296	1.47E-22
Mlec	7.23E-27	0.276388607	0.416	0.158	1.53E-22
9530068E07Rik	7.29E-27	0.30387292	0.525	0.22	1.55E-22
Rarres2	8.21E-27	0.514767519	0.928	0.681	1.74E-22
C1s1	1.08E-26	0.442807487	0.803	0.431	2.28E-22
Cpne3	1.12E-26	0.352189191	0.637	0.286	2.38E-22
Psma6	1.14E-26	0.294418644	0.669	0.303	2.42E-22
Son	1.22E-26	0.335114091	0.588	0.258	2.59E-22
Atp1a1	1.24E-26	0.295356649	0.522	0.213	2.62E-22
Etfl	1.31E-26	0.280156947	0.5	0.2	2.78E-22

Irgm1	1.50E-26	0.545209523	0.312	0.109	3.19E-22
Grina	2.27E-26	0.324275102	0.478	0.195	4.81E-22
H2afy	2.99E-26	0.263729139	0.5	0.203	6.33E-22
Set	4.24E-26	0.379011493	0.669	0.317	9.00E-22
Cdk2ap2	4.63E-26	0.289519138	0.522	0.22	9.81E-22
H2-T23	4.66E-26	0.276939457	0.444	0.175	9.88E-22
Ctsb	1.22E-25	0.482520824	0.856	0.509	2.58E-21
Fabp5	1.29E-25	0.391819987	0.588	0.264	2.73E-21
Selenok	1.60E-25	0.433507766	0.741	0.399	3.39E-21
H2afv	1.70E-25	0.289746216	0.556	0.239	3.61E-21
Idi1	1.98E-25	0.420254235	0.578	0.265	4.19E-21
Nckap1	2.59E-25	0.265004215	0.456	0.182	5.49E-21
Gdf15	2.82E-25	0.333109424	0.297	0.102	5.98E-21
Eef1g	3.02E-25	0.316655071	0.656	0.304	6.40E-21
Apoa4	3.04E-25	0.485599191	0.503	0.213	6.45E-21
Atp6v0b	3.52E-25	0.3281834	0.556	0.249	7.46E-21
Bhlhe40	3.77E-25	0.292807131	0.584	0.257	8.00E-21
Psma1	3.90E-25	0.323986037	0.65	0.302	8.27E-21
Stat3	4.03E-25	0.254969112	0.438	0.172	8.54E-21
Bst2	4.13E-25	0.477623567	0.772	0.442	8.76E-21
Cbr1	5.37E-25	0.272513133	0.472	0.192	1.14E-20
Ostc	7.32E-25	0.338895903	0.603	0.279	1.55E-20
Rnf130	8.93E-25	0.273503271	0.412	0.162	1.89E-20
Rbx1	1.24E-24	0.315255474	0.637	0.3	2.63E-20
Ctsh	1.66E-24	0.415286619	0.738	0.369	3.52E-20
Klhl24	1.74E-24	0.262349082	0.522	0.222	3.68E-20
Arhgef12	2.07E-24	0.282546777	0.528	0.228	4.39E-20
F2	2.66E-24	0.466086528	0.953	0.754	5.63E-20
Apoh	2.92E-24	0.388318616	0.978	0.911	6.19E-20
Rpn1	2.92E-24	0.37822827	0.688	0.339	6.20E-20
Ctsd	3.10E-24	0.334325225	0.681	0.326	6.57E-20
Ddah1	3.67E-24	0.42403604	0.672	0.331	7.79E-20
Clta	4.25E-24	0.338209515	0.669	0.328	9.00E-20
Tcp1	4.47E-24	0.265513666	0.534	0.234	9.47E-20
Pter	8.33E-24	0.346644816	0.547	0.246	1.77E-19
Sumo2	2.34E-23	0.373648741	0.684	0.351	4.97E-19
Hpn	3.18E-23	0.395617256	0.706	0.372	6.75E-19
H3f3b	3.52E-23	0.466864178	0.912	0.675	7.47E-19
Lpgat1	3.85E-23	0.36742834	0.759	0.388	8.17E-19
Nr2f6	4.40E-23	0.26536372	0.55	0.245	9.33E-19
Hmgcr	1.14E-22	0.401085757	0.409	0.169	2.42E-18
Tmed10	2.37E-22	0.383316083	0.741	0.399	5.02E-18
Gstm2	4.28E-22	0.272534996	0.284	0.101	9.07E-18

Kif1b	5.31E-22	0.276266447	0.522	0.236	1.12E-17
Prox1	5.97E-22	0.333670415	0.556	0.263	1.27E-17
Cd81	6.31E-22	0.510842804	0.863	0.575	1.34E-17
Hnrnpu	6.47E-22	0.335897576	0.691	0.352	1.37E-17
Npm1	9.64E-22	0.456339738	0.787	0.481	2.04E-17
Ywhaq	1.03E-21	0.269809244	0.55	0.255	2.19E-17
Slc6a13	1.47E-21	0.282952281	0.572	0.266	3.12E-17
Prdx2	2.01E-21	0.377681366	0.7	0.389	4.26E-17
Lamp1	2.57E-21	0.468347948	0.919	0.687	5.45E-17
Osgin1	2.83E-21	0.286033164	0.444	0.193	5.99E-17
Rrbp1	3.01E-21	0.447205029	0.769	0.448	6.39E-17
Rpl5	5.08E-21	0.489706844	0.8	0.54	1.08E-16
Zfand5	5.53E-21	0.257161987	0.503	0.228	1.17E-16
Rpl7	6.73E-21	0.451847351	0.922	0.729	1.43E-16
Eif4a1	7.23E-21	0.394445341	0.784	0.465	1.53E-16
Arf1	8.42E-21	0.406887578	0.659	0.354	1.79E-16
Dad1	1.56E-20	0.355051585	0.756	0.418	3.30E-16
Mtdh	2.02E-20	0.268989226	0.562	0.265	4.27E-16
Dstn	3.54E-20	0.415759764	0.731	0.421	7.51E-16
Atp6v1g1	4.96E-20	0.311609552	0.706	0.383	1.05E-15
Spcs2	5.38E-20	0.37483101	0.731	0.417	1.14E-15
Pfn1	7.83E-20	0.379629393	0.853	0.557	1.66E-15
Hnrnpab	7.99E-20	0.258363865	0.581	0.279	1.69E-15
Ran	9.63E-20	0.417178169	0.703	0.39	2.04E-15
Id2	1.09E-19	0.4603996	0.725	0.415	2.31E-15
Rora	1.47E-19	0.321402556	0.634	0.33	3.12E-15
Fgg	2.01E-19	0.472831624	1	0.97	4.26E-15
Hdgf	2.25E-19	0.258855073	0.662	0.332	4.77E-15
Atxn7l3b	2.66E-19	0.304730607	0.631	0.318	5.63E-15
Pdia4	3.16E-19	0.295904926	0.644	0.322	6.70E-15
Tkfc	3.52E-19	0.286593311	0.619	0.312	7.45E-15
Sec61a1	3.66E-19	0.271617962	0.531	0.251	7.75E-15
Mrfap1	6.19E-19	0.258253225	0.691	0.361	1.31E-14
Sh3bgrl	8.73E-19	0.268484054	0.653	0.33	1.85E-14
Fads1	1.12E-18	0.302933943	0.713	0.373	2.37E-14
Btf3	1.13E-18	0.399705373	0.816	0.551	2.39E-14
H3f3a	1.48E-18	0.37639386	0.906	0.667	3.13E-14
Ndufb6	1.48E-18	0.280523086	0.75	0.407	3.14E-14
Cald1	1.57E-18	0.388713422	0.875	0.57	3.32E-14
Mbl1	2.44E-18	0.275259026	0.787	0.427	5.17E-14
Tmbim6	3.00E-18	0.392263923	0.947	0.749	6.35E-14
Tor1aip2	3.54E-18	0.284893844	0.484	0.231	7.50E-14
Hnrnpa2b1	4.38E-18	0.397314221	0.841	0.545	9.29E-14

Elob	5.61E-18	0.275839021	0.816	0.464	1.19E-13
Entpd5	6.39E-18	0.252861764	0.484	0.228	1.36E-13
Tpi1	6.86E-18	0.30962483	0.762	0.427	1.46E-13
Dbi	7.46E-18	0.278916315	0.997	0.967	1.58E-13
Surf4	1.31E-17	0.304947801	0.609	0.318	2.77E-13
Aldh1a7	1.47E-17	0.2982854	0.669	0.355	3.11E-13
Rnf11	2.11E-17	0.2607517	0.644	0.337	4.48E-13
Trp53inp1	2.96E-17	0.367881629	0.566	0.293	6.28E-13
Agpat2	3.12E-17	0.308822209	0.8	0.472	6.62E-13
Akr1a1	3.60E-17	0.307175755	0.784	0.495	7.63E-13
Lbp	3.66E-17	0.254199332	0.431	0.2	7.76E-13
Lipa	6.22E-17	0.343216994	0.728	0.409	1.32E-12
C4b	8.68E-17	0.366525121	0.853	0.552	1.84E-12
Creg1	1.05E-16	0.453832838	0.853	0.579	2.22E-12
Ptp4a2	1.13E-16	0.281392298	0.659	0.356	2.39E-12
Rpn2	1.30E-16	0.2920571	0.581	0.296	2.75E-12
Rpsa	1.34E-16	0.351790561	0.966	0.829	2.84E-12
Sppl2a	1.49E-16	0.317183247	0.772	0.445	3.17E-12
Itm2b	1.67E-16	0.301921227	0.991	0.909	3.55E-12
Rplp0	1.87E-16	0.359705939	0.922	0.74	3.97E-12
Selenos	2.20E-16	0.285601437	0.566	0.296	4.66E-12
Ldha	2.30E-16	0.408776025	0.909	0.678	4.88E-12
Tmem59	2.52E-16	0.316849818	0.775	0.451	5.35E-12
Hspa5	2.69E-16	0.42994662	0.941	0.759	5.69E-12
Acsl5	3.04E-16	0.278855991	0.584	0.305	6.45E-12
Tbca	3.52E-16	0.32263173	0.825	0.512	7.46E-12
Bsg	4.60E-16	0.367447779	0.816	0.539	9.76E-12
Agt	4.62E-16	0.391749486	0.8	0.499	9.80E-12
Rpl15	4.79E-16	0.374290947	0.916	0.753	1.01E-11
Plin2	1.39E-15	0.280001614	0.809	0.496	2.94E-11
Ddx5	1.94E-15	0.332137278	0.856	0.567	4.11E-11
Vmp1	2.72E-15	0.273125245	0.709	0.393	5.77E-11
Ppib	6.33E-15	0.309015515	0.834	0.532	1.34E-10
Rps3	1.32E-14	0.32715143	0.878	0.659	2.80E-10
Mif	1.33E-14	0.283443331	0.838	0.542	2.82E-10
Serpinf2	1.69E-14	0.319198733	0.856	0.548	3.58E-10
Eef1b2	2.06E-14	0.328366148	0.809	0.536	4.37E-10
Hnrnpa3	2.73E-14	0.266355128	0.684	0.392	5.79E-10
Gpt2	3.25E-14	0.302098714	0.794	0.483	6.90E-10
Iigp1	4.29E-14	0.64245753	0.922	0.638	9.09E-10
Naca	7.18E-14	0.291634054	0.856	0.667	1.52E-09
Ndufc2	9.11E-14	0.279356533	0.809	0.503	1.93E-09
Aadac	1.61E-13	0.313821232	0.816	0.528	3.42E-09

Pcbp2	2.36E-13	0.296198036	0.809	0.527	4.99E-09
Rpl6	3.10E-13	0.305347556	0.881	0.694	6.58E-09
Serpind1	5.38E-13	0.252586875	0.762	0.465	1.14E-08
Canx	6.63E-13	0.287991658	0.922	0.662	1.41E-08
Rpl10a	8.70E-13	0.314822207	0.925	0.759	1.84E-08
Rack1	1.04E-12	0.295993535	0.881	0.653	2.21E-08
Neat1	1.67E-12	0.321464764	0.884	0.622	3.55E-08
Calm1	1.80E-12	0.267884005	0.812	0.539	3.82E-08
Rps27a	1.86E-12	0.2548295	0.981	0.915	3.95E-08
Dnaja1	2.78E-12	0.267444973	0.831	0.558	5.89E-08
Apom	2.93E-12	0.307378715	0.856	0.596	6.21E-08
S100a10	3.58E-12	0.301880922	0.734	0.466	7.58E-08
Sc5d	7.95E-12	0.312012581	0.809	0.543	1.69E-07
C8a	8.03E-12	0.310993159	0.881	0.61	1.70E-07
Eef2	8.27E-12	0.36620411	0.897	0.72	1.75E-07
Sult1a1	2.66E-11	0.261214993	0.672	0.425	5.64E-07
Zfp36l1	6.05E-11	0.284073079	0.841	0.589	1.28E-06
Arl6ip1	2.58E-10	0.331769333	0.769	0.488	5.47E-06
Orm1	4.07E-10	0.498447146	0.963	0.946	8.63E-06
Apof	4.15E-10	0.28293409	0.878	0.67	8.79E-06
Ces1g	1.20E-09	0.323883701	0.681	0.456	2.54E-05
Rps16	4.04E-09	0.265889953	0.953	0.863	8.55E-05
Gclc	1.71E-07	0.293582322	0.828	0.574	0.003618095

Table S4□ KEGG enrichment analysis of cluster 7's DEGs

Description	GeneRatio	BgRatio	pvalue	p.adjust	qvalue	Count
Complement and coagulation cascades	22/438	93/8912	4.59E-10	1.37E-07	9.80E-08	22
Phagosome	31/438	182/8912	9.25E-10	1.38E-07	9.88E-08	31
Ferroptosis	14/438	40/8912	2.80E-09	2.79E-07	1.99E-07	14
Protein processing in endoplasmic reticulum	28/438	172/8912	1.73E-08	1.30E-06	9.26E-07	28
Fluid shear stress and atherosclerosis	25/438	148/8912	4.85E-08	2.90E-06	2.07E-06	25
Salmonella infection	33/438	253/8912	2.34E-07	1.17E-05	8.34E-06	33
Antigen processing and presentation	18/438	90/8912	2.82E-07	1.20E-05	8.61E-06	18
Lysosome	22/438	131/8912	3.47E-07	1.30E-05	9.28E-06	22
Coronavirus disease - COVID-19	32/438	247/8912	4.19E-07	1.39E-05	9.95E-06	32
Human cytomegalovirus infection	31/438	256/8912	2.77E-06	8.27E-05	5.91E-05	31
Pertussis	15/438	77/8912	3.94E-06	0.000107	7.66E-05	15
Kaposi sarcoma-associated herpesvirus infection	27/438	224/8912	1.34E-05	0.000333	0.000238	27
Steroid biosynthesis	7/438	20/8912	2.93E-05	0.000674	0.000481	7
Adherens junction	13/438	71/8912	3.49E-05	0.000744	0.000532	13
Glutathione metabolism	13/438	72/8912	4.07E-05	0.000811	0.000579	13
Lipid and atherosclerosis	25/438	216/8912	5.54E-05	0.001035	0.00074	25
Terpenoid backbone biosynthesis	7/438	23/8912	8.14E-05	0.001432	0.001024	7
Cholesterol metabolism	10/438	49/8912	0.000108	0.001761	0.001258	10
Apoptosis	18/438	136/8912	0.000112	0.001761	0.001258	18
Platinum drug resistance	13/438	80/8912	0.000126	0.001888	0.001349	13
Metabolism of xenobiotics by cytochrome P450	12/438	73/8912	0.000204	0.002908	0.002078	12
Spliceosome	17/438	134/8912	0.000289	0.003851	0.002752	17
Toxoplasmosis	15/438	110/8912	0.000296	0.003851	0.002752	15
Hepatocellular carcinoma	20/438	174/8912	0.000334	0.00398	0.002844	20
Arrhythmogenic right ventricular cardiomyopathy	12/438	77/8912	0.000342	0.00398	0.002844	12
Thyroid cancer	8/438	37/8912	0.00035	0.00398	0.002844	8
Viral carcinogenesis	24/438	229/8912	0.000359	0.00398	0.002844	24
Human papillomavirus infection	33/438	362/8912	0.000424	0.00453	0.003237	33
Hepatitis C	19/438	165/8912	0.000457	0.004612	0.003296	19
Human T-cell leukemia virus 1 infection	25/438	247/8912	0.000463	0.004612	0.003296	25
Regulation of actin cytoskeleton	23/438	220/8912	0.000491	0.00474	0.003387	23
Tight junction	19/438	167/8912	0.000531	0.004965	0.003549	19
Leishmaniasis	11/438	70/8912	0.000557	0.00505	0.003609	11
Human immunodeficiency virus 1 infection	24/438	240/8912	0.000712	0.006258	0.004472	24
Chemical carcinogenesis - DNA adducts	12/438	84/8912	0.00077	0.006575	0.004699	12
Bacterial invasion of epithelial cells	11/438	76/8912	0.001132	0.009146	0.006537	11
Pancreatic cancer	11/438	76/8912	0.001132	0.009146	0.006537	11
Parkinson disease	25/438	264/8912	0.001222	0.009619	0.006874	25

AGE-RAGE signaling pathway in diabetic complications	13/438	101/8912	0.00128	0.009815	0.007014	13
Tuberculosis	19/438	180/8912	0.001327	0.009917	0.007088	19
Chemical carcinogenesis - receptor activation	22/438	225/8912	0.001571	0.011458	0.008189	22
Fatty acid biosynthesis	5/438	19/8912	0.001837	0.012868	0.009196	5
Proteasome	8/438	47/8912	0.001851	0.012868	0.009196	8
Epstein-Barr virus infection	22/438	231/8912	0.002196	0.014923	0.010665	22
Drug metabolism - cytochrome P450	10/438	71/8912	0.002317	0.015392	0.011	10
Neurotrophin signaling pathway	14/438	121/8912	0.002381	0.015474	0.011059	14
Proteoglycans in cancer	20/438	205/8912	0.002593	0.016495	0.011788	20
Fatty acid metabolism	9/438	62/8912	0.003072	0.019134	0.013674	9
Prion disease	24/438	268/8912	0.003192	0.019476	0.013918	24
Bile secretion	12/438	100/8912	0.003524	0.021075	0.015062	12
ECM-receptor interaction	11/438	88/8912	0.003731	0.021876	0.015634	11
Cellular senescence	18/438	184/8912	0.004046	0.023265	0.016627	18
Amyotrophic lateral sclerosis	30/438	369/8912	0.004473	0.025236	0.018035	30
Hypertrophic cardiomyopathy	11/438	91/8912	0.004837	0.026785	0.019142	11
Leukocyte transendothelial migration	13/438	118/8912	0.005131	0.027894	0.019935	13
Drug metabolism - other enzymes	11/438	92/8912	0.005259	0.028079	0.020067	11
Small cell lung cancer	11/438	93/8912	0.005709	0.029947	0.021402	11
Dilated cardiomyopathy	11/438	94/8912	0.006189	0.031798	0.022725	11
Hepatitis B	16/438	163/8912	0.006325	0.031798	0.022725	16
Chemical carcinogenesis - reactive oxygen species	20/438	222/8912	0.006381	0.031798	0.022725	20
Endometrial cancer	8/438	58/8912	0.007047	0.034544	0.024688	8
Alzheimer disease	30/438	383/8912	0.007548	0.036398	0.026013	30
Legionellosis	8/438	61/8912	0.00953	0.045229	0.032324	8
Focal adhesion	18/438	201/8912	0.009968	0.046038	0.032902	18
HIF-1 signaling pathway	12/438	114/8912	0.010008	0.046038	0.032902	12
PI3K-Akt signaling pathway	28/438	359/8912	0.010222	0.046309	0.033095	28
Viral myocarditis	10/438	88/8912	0.010814	0.048259	0.034489	10

Supplementary reference

1. Koo JH, Lee HJ, Kim W, Kim SG. Endoplasmic Reticulum Stress in Hepatic Stellate Cells Promotes Liver Fibrosis via PERK-Mediated Degradation of HNRNPA1 and Up-regulation of SMAD2. Gastroenterology. 2016 Jan;150(1):181-93 e8.